Table III. Continued.

| Gene symbol | Description | Gene expression ($log_2$ tumor/normal ratio) | | | | Biological process |
|---|---|---|---|---|---|---|
| | | 13T/13N | 15T/13N | 17T/13N | Pheo/ normal | |
| Pdgfra | Platelet-derived growth factor receptor α polypeptide | -2.13 | -3.83 | -4.69 | -4.61 | Cell proliferation |
| Prlr | Prolactin receptor | -2.36 | -4.45 | -4.63 | -3.46 | Steroid biosynthetic process |
| Rgn | Regucalcin | -4.31 | -3.35 | -6.08 | -5.15 | |
| Rnf43 | Ring finger protein 43 | -2.58 | -4.67 | -6.19 | -4.94 | |
| Scarb1 | Scavenger receptor class B, member 1 | -2.13 | -5.29 | -5.83 | -5.53 | Cholesterol metabolic process |
| Sec14l4 | SEC14-like 4 | -2.44 | -3.45 | -6.50 | -3.53 | Transport |
| Slc37a2 | Solute carrier family 37, member 2 | -2.19 | -3.17 | -3.77 | -4.60 | Transport |
| Soat1 | Sterol O-acyltransferase 1 | -2.72 | -4.95 | -5.38 | -4.39 | Lipid metabolic process |
| Star | Steroidogenic acute regulator, nuclear gene encoding mitochondrial protein | -1.73 | -6.67 | -8.63 | -8.64 | Steroid biosynthetic process |
| Steap4 | STEAP family member 4 | -1.68 | -2.51 | -3.96 | -3.50 | Electron transport |
| Tbx3 | T-box 3 | -1.86 | -4.69 | -5.22 | -4.77 | Anti-apoptosis |
| Tcf21 | Transcription factor 21 | -2.07 | -2.76 | -5.20 | -3.88 | Organ morphogenesis |
| Tspan12 | Tetraspanin 12 | -2.09 | -4.89 | -5.29 | -3.49 | |
| Tst | Thiosulfate sulfurtransferase | -2.44 | -4.79 | -5.00 | -4.70 | Sulfate transport |
| Wnt4 | Wingless-type MMTV integration site family, member 4 | -2.86 | -7.27 | -7.73 | -3.78 | Multicellular organismal development |

Pheo, human pheochromocytoma; normal, human normal adrenal medulla.

human cancers (26). In hematoxylin and eosin-stained sections, mouse adrenal tumor was composed of undifferentiated cells with a large nucleus (Fig. 1M and N). From comparison of the gene expression profiles by hierarchical clustering, up- or down-regulated genes in mouse adrenal tumor were overall similar to those in human pheochromocytoma (Fig. 3), but the expression patterns of noradrenergic neuron-related genes in mouse adrenal tumor were dissimilar with those in human pheochromocytoma (Table I), indicating that the characterization of mouse adrenal tumor was similar to that of human adrenal neuroblastoma rather than pheochromocytoma. This transgenic mouse might be a useful model of undifferentiated and aggressive adrenal neuroblastoma.

Researchers are studying chemotherapy drugs in order to find an effective therapy for neuroblastoma. In chemotherapy for high-risk neuroblastoma, the following drugs are often used: cyclophosphamide, ifosfamide, cisplatin, carboplatin, vincristine, doxorubicin (DXR), melphalan, etoposide (VP-16), teniposide (VM-26), and topotecan. In this study, we found that the expression of DNA topoisomerase II (Topo IIα) mRNA in adrenal tumors of transgenic mice increased 120-150-fold compared to non-transgenic mice (data not shown); therefore, we investigated the antitumor effect for transgenic mice by DXR, which is an inhibitor of Topo IIα. As a result, i.v. administration of DXR could suppress tumor growth significantly (data not shown), corresponding with the prognostic results from DNA array; therefore, this mouse model would be a useful tool for the development of anti-cancer drugs of neuroblastoma.

## Acknowledgements

This study was supported in part by a Grant-in-Aid for Scientific Research from the Ministry of Education, Culture, Sports, Science, and Technology of Japan, and by the Open Research Center Project.

## References

1. Brodeur GM, Maris JM, Yamashiro DJ, Hogarty MD and White PS: Biology and genetics of human neuroblastomas. J Pediatr Hematol Oncol 19: 93-101, 1997.
2. Yamamoto K, Hanada R, Kikuchi A, *et al*: Spontaneous regression of localized neuroblastoma detected by mass screening. J Clin Oncol 16: 1265-1269, 1998.
3. Tischler AS: Pheochromocytoma and extra-adrenal paraganglioma: updates. Arch Pathol Lab Med 132: 1272-1284, 2008.
4. Adler JT, Meyer-Rochow GY, Chen H, *et al*: Pheochromocytoma: current approaches and future directions. Oncologist 13: 779-793, 2008.

5. Aguzzi A, Wagner EF, Williams RL and Courtneidge SA: Sympathetic hyperplasia and neuroblastomas in transgenic mice expressing polyoma middle T antigen. New Biol 2: 533-543, 1990.
6. Hammang JP, Baetge EE, Behringer RR, Brinster RL, Palmiter RD and Messing A: Immortalized retinal neurons derived from SV40 T-antigen-induced tumors in transgenic mice. Neuron 4: 775-782, 1990.
7. Helseth A, Siegal GP, Haug E and Bautch VL: Transgenic mice that develop pituitary tumors: a model for Cushing's disease. Am J Pathol 140: 1071-1080, 1992.
8. Suri C, Fung BP, Tischler AS and Chikaraishi DM: Catecholaminergic cell lines from the brain and adrenal glands of tyrosine hydroxylase-SV40 T antigen transgenic mice. J Neurosci 13: 1280-1291, 1993.
9. Fung KM, Chikaraishi DM, Suri C, *et al*: Molecular phenotype of simian virus 40 large T antigen-induced primitive neuroectodermal tumors in four different lines of transgenic mice. Lab Invest 70: 114-124, 1994.
10. Schulz N, Propst F, Rosenberg MM, *et al*: Patterns of neoplasia in c-mos transgenic mice and their relevance to multiple endocrine neoplasia. Henry Ford Hosp Med J 40: 307-311, 1992.
11. Schulz N, Propst F, Rosenberg MP, *et al*: Pheochromocytomas and C-cell thyroid neoplasms in transgenic c-mos mice: a model for the human multiple endocrine neoplasia type 2 syndrome. Cancer Res 52: 450-455, 1992.
12. Smith-Hicks CL, Sizer KC, Powers JF, Tischler AS and Costantini F: C-cell hyperplasia, pheochromocytoma and sympathoadrenal malformation in a mouse model of multiple endocrine neoplasia type 2B. EMBO J 19: 612-622, 2000.
13. Williams BO, Schmitt EM, Remington L, *et al*: Extensive contribution of Rb-deficient cells to adult chimeric mice with limited histopathological consequences. EMBO J 13: 4251-4259, 1994.
14. You MJ, Castrillon DH, Bastian BC, *et al*: Genetic analysis of Pten and Ink4a/Arf interactions in the suppression of tumorigenesis in mice. Proc Natl Acad Sci USA 99: 1455-1460, 2002.
15. Jacks T, Shih TS, Schmitt EM, Bronson RT, Bernards A and Weinberg RA: Tumour predisposition in mice heterozygous for a targeted mutation in Nf1. Nat Genet 7: 353-361, 1994.
16. Iwakura H, Ariyasu H, Kanamoto N, *et al*: Establishment of a novel neuroblastoma mouse model. Int J Oncol 33: 1195-1199, 2008.
17. Hattori Y and Maitani Y: Folate-linked nanoparticle-mediated suicide gene therapy in human prostate cancer and nasopharyngeal cancer with herpes simplex virus thymidine kinase. Cancer Gene Ther 12: 796-809, 2005.
18. Wong DL: Why is the adrenal adrenergic? Endocr Pathol 14: 25-36, 2003.
19. Tischler AS, Freund R, Carroll J, *et al*: Polyoma-induced neoplasms of the mouse adrenal medulla. Characterization of the tumors and establishment of cell lines. Lab Invest 68: 541-549, 1993.
20. Cheung IY, Feng Y, Gerald W and Cheung NK: Exploiting gene expression profiling to identify novel minimal residual disease markers of neuroblastoma. Clin Cancer Res 14: 7020-7027, 2008.
21. Moreno-Sanchez R, Rodriguez-Enriquez S, Marin-Hernandez A and Saavedra E: Energy metabolism in tumor cells. FEBS J 274: 1393-1418, 2007.
22. Nakata H and Kozasa T: Functional characterization of Galphao signaling through G protein-regulated inducer of neurite outgrowth 1. Mol Pharmacol 67: 695-702, 2005.
23. Hedborg F, Ohlsson R, Sandstedt B, Grimelius L, Hoehner JC and Pahlman S: IGF2 expression is a marker for paragaglionic/SIF cell differentiation in neuroblastoma. Am J Pathol 146: 833-847, 1995.
24. Swerts K, De MB, Dhooge C, *et al*: Potential application of ELAVL4 real-time quantitative reverse transcription-PCR for detection of disseminated neuroblastoma cells. Clin Chem 52: 438-445, 2006.
25. Zhou J, Li J, Chen J, Liu Y, Gao W and Ding Y: Over-expression of CDH22 is associated with tumor progression in colorectal cancer. Tumour Biol 30: 130-140, 2009.
26. Deeb KK, Michalowska AM, Yoon CY, *et al*: Identification of an integrated SV40 T/t-antigen cancer signature in aggressive human breast, prostate, and lung carcinomas with poor prognosis. Cancer Res 67: 8065-8080, 2007.

Cancer Science
The official journal of the Japanese Cancer Association

# Enhanced antitumor efficacy of folate-linked liposomal doxorubicin with TGF-β type I receptor inhibitor

Yukimi Taniguchi,[1] Kumi Kawano,[1] Takuya Minowa,[1] Takashi Sugino,[2] Yuki Shimojo[1] and Yoshie Maitani[1,3]

[1]Institute of Medicinal Chemistry, Hoshi University, Tokyo; [2]Department of Basic Pathology, Fukushima Medical University, Fukushima City, Japan

(Received March 18, 2010/Revised May 24, 2010/Accepted June 3, 2010/Accepted manuscript online June 14, 2010/Article first published online July 1, 2010)

**Tumor cell targeting of drug carriers is a promising strategy and uses the attachment of various ligands to enhance the therapeutic potential of chemotherapy agents. Folic acid is a high-affinity ligand for folate receptor, which is a functional tumor-specific receptor. The transforming growth factor (TGF)-β type I receptor (TβR-I) inhibitor A-83-01 was expected to enhance the accumulation of nanocarriers in tumors by changing the microvascular environment. To enhance the therapeutic effect of folate-linked liposomal doxorubicin (F-SL), we co-administrated F-SL with A-83-01. Intraperitoneally injected A-83-01-induced alterations in the cancer-associated neovasculature were examined by magnetic resonance imaging (MRI) and histological analysis. The targeting efficacy of single intravenous injections of F-SL combined with A-83-01 was evaluated by measurement of the biodistribution and the antitumor effect in mice bearing murine lung carcinoma M109. A-83-01 temporarily changed the tumor vasculature around 3 h post injection. A-83-01 induced 1.7-fold higher drug accumulation of F-SL in the tumor than liposome alone at 24 h post injection. Moreover F-SL co-administrated with A-83-01 showed significantly greater antitumor activity than F-SL alone. This study shows that co-administration of TβR-I inhibitor will open a new strategy for the use of FR-targeting nanocarriers for cancer treatment. (*Cancer Sci* 2010; 101: 2207–2213)**

Polyethylene glycol (PEG)-modified nanocarriers are long-lived in the circulation and accumulate passively in tumors. To enhance the selection of target cells within the tumor site, a variety of targeting ligands have been examined in tumor-targeting drug carriers. Folate receptor (FR)-α is a glycosyl phosphatidylinositol (GPI)-anchored membrane protein that is selectively overexpressed in over 90% of ovarian carcinomas[1,2] and to various extents in other epithelial cancers but is only minimally distributed in normal tissues.[3–6] Folate receptor (FR) can serve as an excellent tumor marker and as a functional tumor-specific receptor. Folic acid, a high-affinity ligand for FR, retains its receptor-binding and endocytosis properties even if it is covalently linked to a wide variety of molecules. As a result, liposomes conjugated to the folate ligand *via* a PEG spacer have been used to deliver chemotherapeutic agents, oligonucleotides, and markers to FR-bearing tumor cells.[7–10]

In our previous studies, folate-linked liposome loaded doxorubicin (DXR), which was optimized for length of the PEG spacer and folate density (F-SL), showed strong potential *in vitro* compared with non-folate-linked PEGylated liposomes (SL).[11] In addition, F-SL showed a slightly stronger antitumor effect than SL *in vivo* irrespective of high level of accumulation on the endothelial cells of tumors.[11] To reach the FR on the tumor cell surface, F-SL requires extravasation from the blood vessel into the tumor region and to pass through the interstitium space. Therefore, we considered that active targeting by folate modification could be achieved by increasing the delivery of F-SL from the endothelial cells to the tumor cell surface with FR. Antiangiogenesis effects are known to change the tumor vasculature; therefore, this technique has already been applied in combination therapy. Bevacizumab, an antivascular endothelial growth factor (anti-VEGF) antibody was developed for blocking angiogenesis, and it is used clinically with other drugs to improve the efficiency of conventional chemotherapy.

The transforming growth factor (TGF)-β type I receptor (TβR-I) inhibitor LY364947 was reported to increase the antitumor effect of an anticancer drug encapsulated in PEGylated nanocarriers by changing the microenvironment of the vasculature.[12] The roles of TGF-β in cancer biology are complex; TGF-β can suppress or promote tumor growth depending on the type of cancer. Small molecule TβR-I inhibitors have a wide variety effects. The TβR-I inhibitor A-83-01 is one of more potent inhibitors of TβR-I kinase/activin receptor-like kinase (ALK)-5 ($IC_{50}$ = 12 nM)[13] than previously described ALK-5 inhibitors, including LY364947 ($IC_{50}$ = 59 nM).[14] To evaluate effect of TβR-I inhibitor on tumor vasculature *in vivo*, magnetic resonance imaging (MRI) is a powerful method.[15,16] We have reported recently that A-83-01 induced alterations in colon 26 cancer-associated neovasculature in mice using MRI.[17] In this study, we used A-83-01 to enhance extravasation of F-SL from the blood vessels. To the best of our knowledge, combination therapy with TβR-I inhibitor and active targeting carriers, such as folate-linked nanocarriers, has not been reported previously, and this report is the first to examine the antitumor effect of F-SL and A-83-01 in combination therapy.

Here we evaluated the effect of A-83-01 treatment on tumor vasculature using MRI, and then we assessed the FR-targeting effect of F-SL co-administrated with A-83-01 on the biodistribution of drug and antitumor activity in mice bearing murine lung carcinoma M109.

## Materials and Methods

**Materials.** Hydrogenated soybean phosphatidylcholine (HSPC), amino-poly (ethyleneglycol)-distearylphosphatidylethanolamine (amino-$PEG_{5000}$-DSPE; PEG mean molecular weight, 5000), and n-(carbonyl-methoxypolyethyleneglycol)-1, 2-distearyl-sn-glycero-3-phosphoethanolamine ($PEG_{2000}$-DSPE; PEG mean molecular weight, 2000) were purchased from NOF (Tokyo, Japan). Egg phosphatidyl choline (EPC) was a kind of gift from Q.P., Tokyo, Japan. Cholesterol (Ch), DXR hydrochloride, and HPLC grade acetonitrile were purchased from Wako Pure Chemical Industries (Osaka, Japan). A-83-01 (Fig. 1a) and LY364947 were purchased from Sigma-Aldrich Japan (Tokyo, Japan). Hoechst 33342 was purchased from Invitrogen (Carlsbad, CA, USA). Magnevist (Gd-DTPA) was purchased

[3]To whom correspondence should be addressed.
E-mail: yoshie@hoshi.ac.jp

doi: 10.1111/j.1349-7006.2010.01646.x

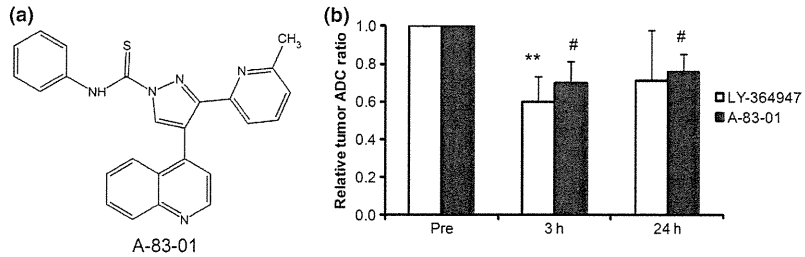


**Fig. 1.** Chemical structure of A-83-01 (a), and the relative apparent diffusion coefficient (ADC) ratio of M109 tumors treated with TβR-I inhibitors compared with pretreatment (Pre) (b). Three or 24 h following intraperitoneal injection of vehicle or TβR-I inhibitor (1 mg LY364947/kg or 0.5 mg A-83-01/kg), diffusion-weighted images were taken. Each value represents the mean ± SD ($n$ = 3). $^{**}P < 0.01$ *versus* LY364947 Pre, $^{\#}P < 0.05$ *versus* A-83-01 Pre.

from Bayer-Schering Pharma (Berlin, Germany). Folate-$PEG_{5000}$-DSPE (F-$PEG_{5000}$-DSPE) was conjugated from folic acid and amino-$PEG_{5000}$-DSPE, which was synthesized as reported previously.[7] Other reagents used in this study were of reagent grade.

**Preparation of folate-linked liposomal DXR.** Liposomes were prepared from HSPC/Ch = 55/45 (mol/mol) by a dry-film method, as described previously.[11] Briefly, all lipids were dissolved in chloroform, which was removed by evaporation. The thin film was hydrated using citrate buffer (300 mM, adjusted to pH 4.0 with NaOH) at 60°C by vortex mixing and sonication. The liposomes were incubated with 2.25 mol% $PEG_{2000}$-DSPE and 0.25 mol% of F-$PEG_{5000}$-DSPE for folate-PEG-liposomes (F-SL), and incubated with 2.5 mol% $PEG_{2000}$-DSPE for PEGylated liposomes (SL) at 60°C for 1 h by the post-insertion technique, and then loaded with DXR by a pH gradient method.[18,19] Doxorubicin (DXR) loading efficiency was determined by separating unencapsulated from encapsulated drug using a Sephadex G-50 column. Doxorubicin (DXR) concentration was determined by measuring absorbance at 480 nm (UV-1700 Phamaspec; Shimadzu, Kyoto, Japan). The resulting mean diameter of liposomes was determined by dynamic light scattering (ELS-Z2; Otsuka Electronics, Osaka, Japan) at 25°C after diluting the liposome suspension with water.

**Preparation of liposomal Gd-DTPA.** Liposomal Gd-DTPA was prepared from EPC/Ch/$PEG_{2000}$-DSPE = 5/2/0.35 (mol/mol) (Gd-L) as described previously.[17] The average particle diameter of liposomes was adjusted to about 120 nm using ultrasound. The relaxation ratio of Gd-L was 4.48 mM/s, which was almost equal to that of Gd-DTPA (4.39 mM/s).[17]

**Animals.** All animal experiments were carried out in accordance with the guidelines of the Guiding Principles for the Care and Use of Laboratory Animals of Hoshi University. Murine lung carcinoma M109 cells (high FR-expressing cell line) were obtained from the Division of Chemotherapy (Translational Research Center), Chiba Cancer Center (Chiba, Japan). The cells were subcultured by employing a biogenic system of BALB/c mice. M109 cells ($1.5 \times 10^6$) were inoculated subcutaneously into CDF1 female mice (5 weeks old, Sankyo Labo Service, Tokyo, Japan).

**Magnetic resonance imaging (MRI).** When the tumor volume reached approximately 100–200 $mm^3$, mice bearing M109 tumors were injected intraperitoneally with A-83-01 or LY364947, at a dose of 0.5 or 1 mg/kg, respectively, using 0.1 mg/mL dissolved in DMSO/saline = 3/2 (v/v, vehicle). Magnetic resonance imaging (MRI) was performed at 3 and 24 h post-injection of A-83-01 or LY364947, compared with pretreatment (''Pre''). Mice were anesthetized using 5% isoflurane (Abbott Japan, Tokyo, Japan) throughout the MRI experiment during their insertion into a 9.4T vertical type MRI (Varian, Palo Alto, CA, USA). High spatial resolution, two-dimensional $T_2$-weighted spin-echo coronal images were acquired to detect the tumor position.

Diffusion-weighted MRI was set by diffusion gradients as described previously.[17] The apparent diffusion coefficient of water in the tumors was calculated and mapped using the following parameters: repetition time (TR) = 2000 ms, echo time (TE) = 45 ms, slice thickness = 3 mm, 64 × 64 data matrix, axial orientation, and field-of-view = 3 × 3 $cm^2$. Three slices through the center of the tumor were acquired.

Dynamic contrast-enhanced (DCE)-MRI acquisition was applied repeatedly to acquire axial slice spoiled gradient-recalled echo images with a second temporal resolution over 6 min: TR = 7.8125 ms, TE = 2.06 ms, matrix resolution = 64 × 64, field of view = 3 × 3 $cm^2$, slice thickness = 4 mm, flip angle = 30°, number of slices = 1, two signal averages as described previously.[17] Gd-DTPA or Gd-L was administered at 0.1 mmol Gd/kg as a bolus with heparinized saline (total volume, ~0.4 mL). With the use of Gd-L, injected lipids containing Gd-L were retained in the tumor; therefore, different mice were used to compare pretreatment with treatment of A-83-01.

Quantitative evaluation of MRI has been described previously.[17] The apparent diffusion coefficient was obtained by the tumor regions of interest transfer to the apparent diffusion coefficient map. The concentration of Gd at each imaging time point in each voxel was obtained from conversion of pixel intensity to absolute concentration values of the contrast agent.[20] The initial area under the tumor Gd concentration-time curve (IAUGC) was calculated at 100 s post injection of contrast agent.

**Immunohistochemical analysis.** When the tumor volume reached approximately 100–200 $mm^3$, A-83-01 was intraperitoneally injected at a dose of 0.5 mg/kg. The mice were sacrificed 3 or 24 h post-injection, and each tumor was resected for A-83-01 treated mice. As a control, the mice were sacrificed 3 h post injection of vehicle, and each tumor was resected as for the untreated mice. Tumors were fixed with 10% formalin for the preparation of paraffin-embedded sections. Immunohistochemistry was performed using monoclonal antibodies against α-smooth muscle actin (Dako, Glostrup, Denmark) to identify pericyte and CD31 (BO Biosciences, San Jose, CA, USA) to detect vascular endothelial cells, in accordance with the manufacturer's protocol.

**Biodistribution studies in tumor-bearing mice.** When the tumor volume reached approximately 100–200 $mm^3$, SL or F-SL was injected intravenously at 5 mg DXR/kg with or without intraperitoneal injection of 0.5 or 1 mg A-83-01/kg. Twenty-four hours post injection of liposomes, the mice were anesthetized by ether inhalation and blood was collected and centrifuged to obtain serum. Then the anesthetized mice were sacrificed, and liver, spleen, kidney, lung, heart, and tumor tissues were collected. Doxorubicin (DXR) levels were determined


doi: 10.1111/j.1349-7006.2010.01646.x

by an HPLC method.[21] The HPLC system was composed of an LC-10AS pump (Shimadzu), a SIL-10A autoinjector (Shimadzu), an RF-10$A_{XL}$ fluorescence detector (Ex, 482 nm, Em, 550 nm; Shimadzu), and an YMC-Pack ODS-A, 150 × 4.6 mm I.D. column (YMC, Kyoto, Japan). The mobile phase was 0.1 M ammonium formate (pH 4.0): acetonitrile = 7:3 (v/v) with a flow rate of 1.0 mL/min. The concentration of DXR in each sample was determined using a calibration curve, with daunomycin as the internal standard.

**Distribution of folate-linked liposomal DXR in solid tumor.** When the tumor volume reached approximately 100–200 $mm^3$, SL or F-SL was injected intravenously at 8 mg DXR/kg with or without intraperitoneal injection of 0.5 mg A-83-01/kg, and then, 24 h post injection of liposomes, the mice were anesthetized by ether inhalation and sacrificed. For the observation of blood vessels, Hoechst 33342, which preferentially stains tumor cells adjacent to blood vessels, was injected intravenously at 7.5 mg/kg in saline 1 min before sacrifice. Tumor tissues were collected and frozen immediately in dry ice. The tumors were embedded in OCT compound and processed by frozen sectioning at 20 μm. Each frozen section was mounted on poly-L-lysine coated slides. The specimens were examined microscopically using an Eclipse TS100 microscope (Nikon, Tokyo, Japan).

**Therapeutic studies.** When the tumor volume reached approximately 100–200 $mm^3$, SL, F-SL, or free DXR was injected intravenously at 8 mg/kg, with or without intraperitoneal injection of 0.5 mg A-83-01/kg. The control group was injected intravenously with saline (0.2 mL/20 g body weight) with intraperitoneal injection of the vehicle (0.1 mL/20 g body weight). Tumor volumes and body weight were measured at regular intervals. The tumor size was measured with vernier calipers. Tumor volume was calculated using the following equation: volume = $\pi/6$ x $LW^2$, where L is the long diameter and W is the short diameter.

**Statistical analysis.** The statistical significance of the data was evaluated by analysis using Student's *t*-test. $P < 0.05$ was considered significant.

## Results

**Magnetic resonance imaging (MRI) of tumors treated with TβR-I inhibitors.** Folate-linked liposomal doxorubicin (F-SL) and SL exhibited a high loading efficiency of >95% at a drug-to-total lipid ratio of 1:5 (w/w), which corresponded with the previous report.[11] In all cases, the average particle diameter of each liposome was ~120 nm with a narrow, monodisperse distribution. A 1 mg/kg dose of LY364947 was reported to enhance the accumulation of nanocarriers in solid tumors.[22] Because the effect of A-83-01 on M109 tumors has not been reported, we examined the tumor accumulation of SL when intraperitoneal post-injection of A-83-01 at doses of 0.5 and 1 mg/kg. Non-folate-linked PEGylated liposomal doxorubicin (SL) with A-83-01 at both doses 24 h post injection showed no significantly different DXR levels in the tumor ($P > 0.05$) (Fig. S1); therefore, we used A-83-01 at a dose of 0.5 mg/kg in the following experiments.

The effect of A-83-01 injected intraperitoneally on M109 tumor vasculature was evaluated using diffusion-weighted MRI compared with that of LY364947. The average apparent diffusion coefficient values of pretreatment (''Pre'') was 0.033 $mm^2/s$. The relative apparent diffusion coefficient ratio to ''Pre'' values decreased significantly at 3 h post injection of LY364947 (1 mg/kg), and 3 and 24 h post-injection of A-83-01 (0.5 mg/kg) (Fig. 1b). Because the intracellular diffusion rate is

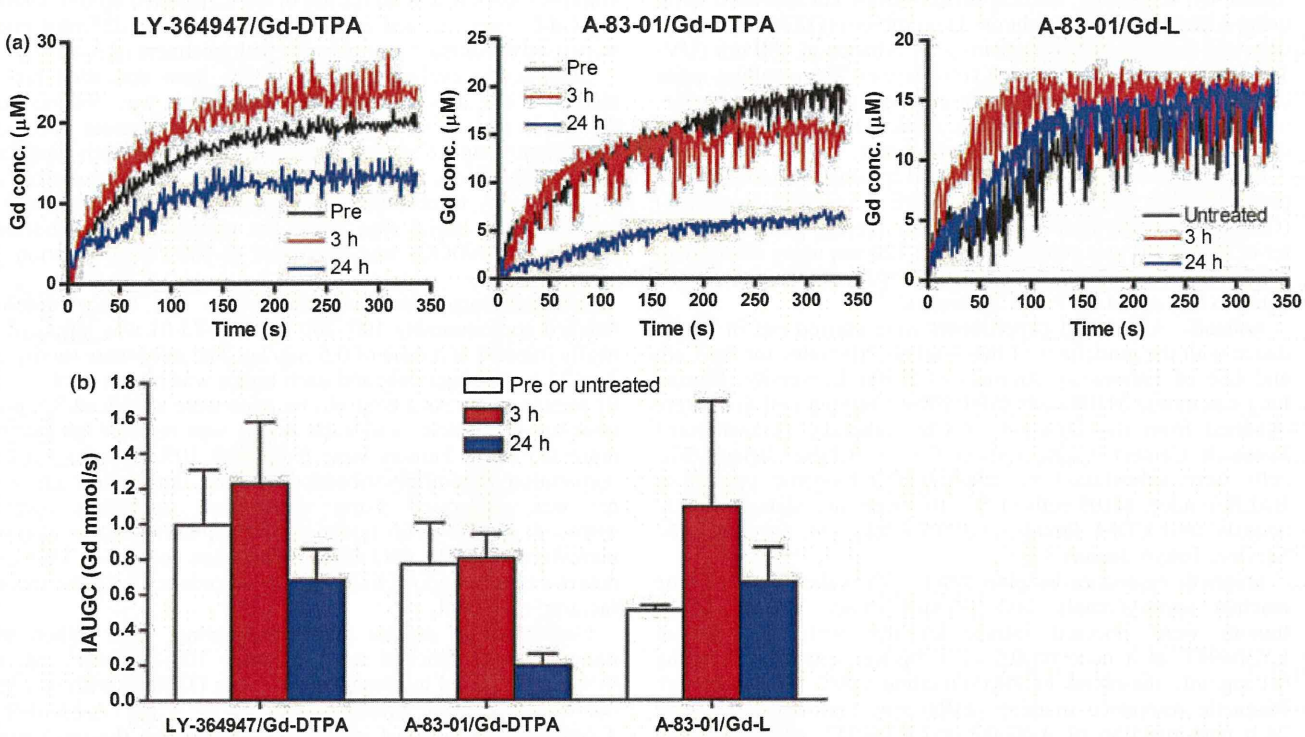


**Fig. 2.** Mean Gd uptake curves in the tumors before (Pre or untreated) and at different time points following intraperitoneal injection of A-83-01 or LY364947 (a), and the area under the Gd concentration curve (IAUGC) from 0 to 100 s postinjection of contrast agent (b). Three or 24 h after intraperitoneal injection of the vehicle or TβR-I inhibitor (1 mg LY364947/kg or 0.5 mg A-83-01/kg), Dynamic contrast-enhanced magnetic resonance imaging (DCE-MRI) was performed using Gd-DTPA for LY364947 and A-83-01 and Gd-L for A-83-01. Each value represents the mean ± SE ($n = 3$).

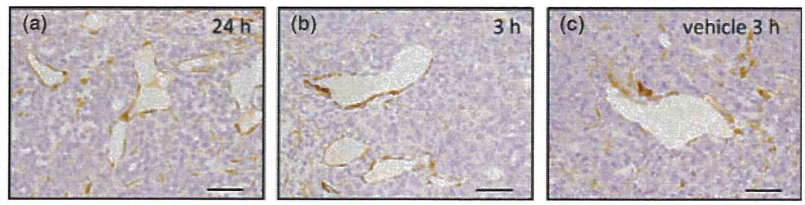


**Fig. 3.** Immunohistochemical analysis of pericyte association with M109 tumor vasculature following treatment with A-83-01. The pericytes lining the intratumoral blood vessels were observed in every tumor treated with A-83-01 (a,b) and vehicle (c). (a) 24 h and (b) 3 h after intraperitoneal injection of A-83-01 at a dose of 0.5 mg/kg. Bar: 50 μm.

one order smaller than that of extracellular water[23], these results suggested that A-83-01 as well as LY364947 decreased the extracellular water and/or increased intracellular water.

In DCE acquisition, a progressive accumulation of Gd-L in the tumor 3 h post injection of A-83-01 was observed during the first 100 s followed by a plateau phase (Fig. 2a). This phenomenon also appeared mice treated with LY364947 using Gd-DTPA for a contrast agent. Gd-L following A-83-01 treatment increased the IAUGC value with a wide error bar at 3 h and then decreased to a similar level to untreated controls at 24 h like Gd-DTPA following LY364947 treatment (Fig. 2b). Gd-DTPA following A-83-01 treatment did not show such an increase in the IAUGC value at 3 h as for LY364947. These results from MRI showed that A-83-01 could change the tumor microenvironment temporarily, resulting in increased IAUGC for Gd-L in the tumor. From this, we decided to co-administrate liposomal DXR with A-83-01 at the same time.

**Immunohistochemical analysis of tumor vasculature treated with A-83-01.** It was reported that TβR-I inhibitor treatment modified the pericyte caverage of tumor neovasculature and influenced on the tumor accumulation of nanocarriers.[12,17] Here, we evaluated the influence of A-83-01 on pericyte association with the tumor neovasculature. The pericyte lining was well conserved in tumors with and without A-83-01, except with scant pericyte association at the periphery in both tumors (Fig. 3). The vasculature-associated pericytes in the treatment group were likely to be slightly more abundant than those of the control (data not shown). These results indicated that A-83-01 did not change markedly pericyte coverage.

**Biodistribution of liposomal DXR with A-83-01.** We examined the influence of A-83-01 on the biodistribution of DXR in mice bearing M109 tumors at 24 h post injection of A-83-01 and liposomal formulations. As shown in Figure 4, in each organ, except in the spleen, serum, and tumor, every group showed similar DXR levels with or without A-83-01. In the spleen, SL with A-83-01 or either F-SL alone or with A-83-01 showed significantly lower DXR levels than SL alone ($P < 0.05$). Similar to the DXR level in the spleen post-injection of SL, A-83-01 greatly decreased the Gd level in the spleen post injection of lipid-nanoparticle containing Gd (Fig. S2). However, the mechanism involved was not clear. In the tumor, SL or F-SL with A-83-01 induced 1.5- or 1.7-fold higher DXR levels, respectively, than that for the liposome alone. Folate-linked liposomal doxorubicin (F-SL) with or without A-83-01 showed significantly higher DXR levels in the tumor than SL alone ($P < 0.05$). This result suggested that among the folate-linked liposomes, F-SL was more effective in tumor accumulation than SL, and A-83-01 enhanced the accumulation of liposomes only in tumors, which was likely to be due to their decrease in the spleen.

**Tumor accumulation of liposomal DXR with A-83-01.** Next, to evaluate the distribution of DXR around the neovasculature in tumors at 24 h following intravenous injection of liposome formulations (8 mg/kg) and intraperitoneal injection of A-83-01, we observed the staining of vessels with Hoechst 33342 using a fluorescence microscope (Fig. 5). Corresponding to the result of the tumor accumulation of DXR in Figure 4, SL or F-SL with A-83-01 showed higher DXR accumulation close to tumor vessels than that for the liposome formulations alone. This result also indicated that A-83-01 enhanced the accumulation of liposomal DXR in tumor vessels as well as in the tumor.

**Antitumor effect of liposomal DXR with A-83-01.** The antitumor effect of F-SL with A-83-01 was evaluated in mice bearing M109 cells. As shown in Figure 6(a), the liposomal DXR injected group showed a strong antitumor effect in comparison with saline with or without A-83-01 and free DXR treated groups. A-83-01 alone did not show an antitumor effect. In the enlargement of the liposomal DXR injected group as shown in Figure 6(b), F-SL with A-83-01 showed a significantly stronger

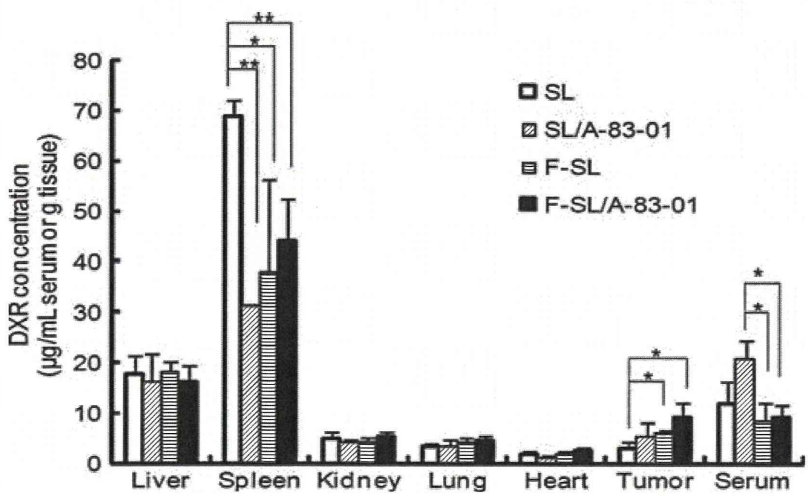


**Fig. 4.** Biodistribution of doxorubicin (DXR) at 24 h after intravenous injection of liposomal DXR (5 mg DXR/kg) with or without intraperitoneal injection of A-83-01 (0.5 mg A-83-01/kg) into CDF1 mice bearing M109 tumors. Each value represents the mean ± SD. ($n = 3$). $^{**}P < 0.01$, $^{*}P < 0.05$.



doi: 10.1111/j.1349-7006.2010.01646.x

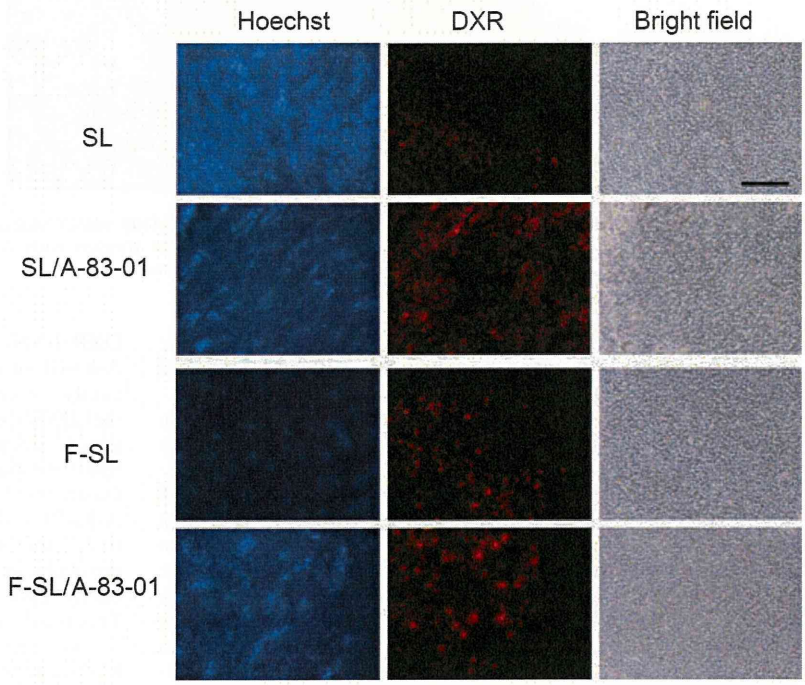


**Fig. 5.** Tumor accumulation of doxorubicin (DXR) in M109 tumors at 24 h after intravenous administration of liposomal DXR at a dose of 8 mg DXR/kg with or without intraperitoneal injection of A-83-01 at a dose of 0.5 mg/kg. Hoechst 33342 was injected into the tail vein 1 min before sacrifice. Then, frozen 20-μm sections were examined by fluorescence microscopy. Bar: 200 μm.

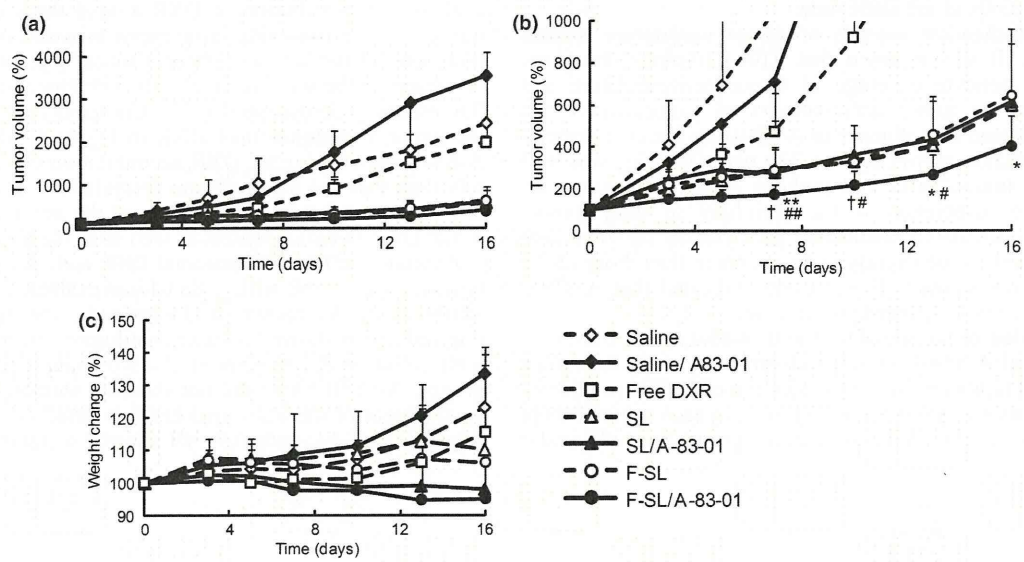


**Fig. 6.** Effects of A-83-01 on the antitumor activity of a single injection of liposomal doxorubicin (DXR) in CDF1 mice bearing M109 tumors. Free DXR, liposomal DXR (8 mg/kg), or saline was administered intravenously in a single bolus with or without intraperitoneal A-83-01 injection (0.5 mg/kg) to mice ($n$ = 6–8). (a) Tumor size; (b) enlargement of (a). (c) Body weight change after drug administration. The formulations used were saline (◇), saline/A-83-01 (♦), free DXR (□), non-folate-linked PEGylated liposomal doxorubicin (SL) (△), SL/A-83-01 (▲), folate-linked liposomal doxorubicin (F-SL) (○), F-SL/A-83-01 (●). #$P < 0.05$, ##$P < 0.01$ *versus* SL, †$P < 0.05$ *versus* SL/A-83-01, *$P < 0.05$, **$P < 0.01$ *versus* F-SL. Each value represents the mean ± SD.

antitumor effect than F-SL alone on day 7 ($P < 0.01$) and days 13 and 16 ($P < 0.05$), SL alone on day 7 ($P < 0.01$) and days 10 and 13 ($P < 0.05$), or SL with A-83-01 on days 7 and 10 ($P < 0.05$). On the other hand, SL with A-83-01 showed a similar antitumor effect to SL or F-SL alone on day 16 ($P > 0.05$). As a result of observation of side-effects of DXR, a tendency of weight loss was not seen post injection of free DXR or liposomal DXR with or without A-83-01 (Fig. 6c). In addition, conspicuous side effects such as diarrhea were not observed in any groups.

## Discussion

In the present study, we demonstrated that A-83-01 enhanced the antitumor effect of F-SL compared with that of F-SL alone in mice bearing M109 tumors. This finding was supported in that A-83-01 induced a temporary high leakiness of Gd-L from the tumor vasculature by means of diffusion-weighted and DCE-MRI, and enhanced the accumulation of liposomal DXR only in tumors.

Here, using liposome-entrapped Gd-DTPA, Gd-L, we could evaluate not only the effect of A-83-01[24] but also estimate the kinetics of liposomal DXR in tumors in combination therapy with A-83-01. Increased IAUGC at 3 h post injection of A-83-01 was inversely related to the apparent diffusion coefficient. These results from MRI showed that A-83-01 could change the tumor microenvironment temporarily, resulting in increased IAUGC of Gd-L in the tumor.

Next, we assessed the FR-targeting effect of F-SL with A-83-01 on the biodistribution of drug and antitumor activity in mice bearing M109 tumors. Under co-administration of A-83-01, F-SL significantly increased the antitumor effect compared with SL on days 7 and 10, whereas F-SL showed slightly higher 24-h accumulation of DXR in the tumor region than SL (Fig. 4). One of the reasons is that the accumulation of F-SL in the tumor may be faster than SL because F-SL exhibited faster clearance compared to SL.[11] In this study, since A-83-01 and liposomal DXR were injected at the same time, A-83-01 will work with early accumulated liposomes in tumors, F-SL more effectively than SL.

Compared with the result of A-83-01 treatment of colon 26 tumors in the previous study[17], the M109 tumor vasculature was more associated with pericytes; therefore, there was no observation of an increase in pericytes 24 h following A-83-01 treatment. In addition, the dose of A-83-01 was decreased from 1 to 0.5 mg/kg because toxicity was increased following injection of DXR. Even in the different tumors and at different doses, A-83-01 increased IAUGC around 3 h post injection and decreased the apparent diffusion coefficient, indicating high levels of Gd permeation from the tumor vasculature to the extracellular space. Tumor angiogenesis is a complex process and dependent on the type of tumors [22], and treatment with TβR-I inhibitor requires a regimen based on the appropriate duration of action. Further optimization of dose and injection time of A-83-01 in combination therapy with folate-linked liposomal anticancer drugs will be needed through evaluation of the microvasculature in tumors using guidance from MRI.

The present results showed that A-83-01 enhanced the accumulation of liposomal DXR only in tumors and showed a significantly stronger antitumor effect of F-SL than of F-SL alone. Further study to optimize the administration schedule of TβR-I inhibitor and F-SL will improve the FR-targeting effect of F-SL.

## Acknowledgments

This work was supported in part by a grant for research on Regulatory Science of Pharmaceuticals and Medical Devices from the Ministry of Health, Labor and Welfare of Japan and by the Open Research Center Project.

## References

1 Weitman SD, Lark RH, Coney LR *et al.* Distribution of the folate receptor GP38 in normal and malignant cell lines and tissues. *Cancer Res* 1992; **52**: 3396–401.
2 Elnakat H, Ratnam M. Distribution functionality and gene regulation of folate receptor isoforms: implications in targeted therapy. *Adv Drug Deliv Rev* 2004; **56**: 1067–84.
3 Wang H, Ross JF, Ratnam M. Structure and regulation of a polymorphic gene encoding folate receptor type gamma/gamma. *Nucleic Acids Res* 1998; **26**: 2132–42.
4 Ross JF, Wang H, Behm FG *et al.* Folate receptor type beta is a neutrophilic lineage marker and is differentially expressed in myeloid leukemia. *Cancer* 1999; **85**: 348–57.
5 Wu M, Gunning W, Ratnam M. Expression of folate receptor type alpha in relation to cell type, malignancy, and differentiation in ovary, uterus, and cervix. *Cancer Epidemiol Biomarkers Prev* 1999; **8**: 775–82.
6 Shen F, Ross JF, Wang X, Ratnam M. Identification of a novel folate receptor, a truncated receptor, and receptor type beta in hematopoietic cells: cDNA cloning, expression, immunoreactivity, and tissue specificity. *Biochemistry* 1994; **33**: 1209–15.
7 Gabizon A, Horowitz AT, Goren D *et al.* Targeting folate receptor with folate linked to extremities of poly(ethylene glycol)-grafted liposomes: *in vitro* studies. *Bioconjug Chem* 1999; **10**: 289–98.
8 Gabizon A, Horowitz AT, Goren D, Tzemach D, Shmeeda H, Zalipsky S. *In vivo* fate of folate-targeted polyethylene-glycol liposomes in tumor-bearing mice. *Clin Cancer Res* 2003; **9**: 6551–9.
9 Pan XQ, Wang H, Lee RJ. Antitumor activity of folate receptor-targeted liposomal doxorubicin in a KB oral carcinoma murine xenograft model. *Pharm Res* 2003; **20**: 417–22.
10 Zhao XB, Lee RJ. Tumor-selective targeted delivery of genes and antisense oligodeoxyribonucleotides via the folate receptor. *Adv Drug Deliv Rev* 2004; **56**: 1193–204.
11 Yamada A, Taniguchi Y, Kawano K, Honda T, Hattori Y, Maitani Y. Design of folate-linked liposomal Doxorubicin to its antitumor effect in mice. *Clin Cancer Res* 2008; **14**: 8161–8.
12 Kano MR, Bae Y, Iwata C *et al.* Improvement of cancer-targeting therapy, using nanocarriers for intractable solid tumors by inhibition of TGF-beta signaling. *Proc Natl Acad Sci USA* 2007; **104**: 3460–5.
13 Tojo M, Hamashima Y, Hanyu A *et al.* The ALK-5 inhibitor A-83-01 inhibits Smad signaling and epithelial-to-mesenchymal transition by transforming growth factor-beta. *Cancer Sci* 2005; **96**: 791–800.
14 Li HY, Wang Y, Heap CR *et al.* Dihydropyrrolopyrazole transforming growth factor-beta type I receptor kinase domain inhibitors: a novel benzimidazole series with selectivity versus transforming growth factor-beta type II receptor kinase and mixed lineage kinase-7. *J Med Chem* 2006; **49**: 2138–42.
15 Tsekos NV, Zhang F, Merkle H, Nagayama M, Iadecola C, Kim SG. Quantitative measurements of cerebral blood flow in rats using the FAIR technique: correlation with previous iodoantipyrine autoradiographic studies. *Magn Reson Med* 1998; **39**: 564–73.
16 O'Connor JP, Jackson A, Parker GJ, Jayson GC. DCE-MRI biomarkers in the clinical evaluation of antiangiogenic and vascular disrupting agents. *Br J Cancer* 2007; **96**: 189–95.
17 Minowa T, Kawano K, Kuribayasi H *et al.* Changes in tumor microenvironment following TGF-beta type I receptor inhibitor treatment observed by diffusion and dynamic contrast-enhanced magnetic resonance imaging. *Br J Cancer* 2009; **101**: 1884–90.
18 Uster PS, Allen TM, Daniel BE, Mendez CJ, Newman MS, Zhu GZ. Insertion of poly(ethylene glycol) derivatized phospholipid into pre-formed liposomes results in prolonged in vivo circulation time. *FEBS Lett* 1996; **386**: 243–6.
19 Lee RJ, Wang S, Turk MJ, Low PS. The effects of pH and intraliposomal buffer strength on the rate of liposome content release and intracellular drug delivery. *Biosci Rep* 1998; **18**: 69–78.
20 Bradley DP, Tessier JJ, Lacey T *et al.* Examining the acute effects of cediranib (RECENTIN, AZD2171) treatment in tumor models: a dynamic contrast-enhanced MRI study using gadopentate. *Magn Reson Imaging* 2009; **27**: 377–84.
21 Matsushita Y, Iguchi H, Kiyosaki T *et al.* A high performance liquid chromatographic method of analysis of 4′-O-tetrahydropyranyladriamycin and their metabolites in biological samples. *J Antibiot (Tokyo)* 1983; **36**: 880–6.
22 Kano MR, Komuta Y, Iwata C *et al.* Comparison of the effects of the kinase inhibitors imatinib, sorafenib, and transforming growth factor-beta receptor inhibitor on extravasation of nanoparticles from neovasculature. *Cancer Sci* 2008; **100**: 173–80.
23 Gass A, Niendorf T, Hirsch JG. Acute and chronic changes of the apparent diffusion coefficient in neurological disorders–biophysical mechanisms and possible underlying histopathology. *J Neurol Sci* 2001; **186**(Suppl 1): S15–23.
24 Turetschek K, Preda A, Novikov V *et al.* Tumor microvascular changes in antiangiogenic treatment: assessment by magnetic resonance contrast media of different molecular weights. *J Magn Reson Imaging* 2004; **20**: 138–44.



doi: 10.1111/j.1349-7006.2010.01646.x

## Supporting Information

Additional supporting information may be found in the online version of this article:

**Fig. S1.** Tumor accumulation of doxorubicin (DXR) in CDF1 mice bearing M109 tumors at 24 h after intravenous administration of non-folate-linked PEGylated liposomal doxorubicin (SL) at a dose of 5 mg DXR/kg with or without intraperitoneal injection of A-83-01 at a dose of 0.5 or 1 mg/kg. Each value represents the mean ± SD ($n$ = 3).

**Fig. S2.** Biodistribution of Gd at 24 h after intravenous injection of lipid-nanoparticle containing Gd (16.3 mg Gd/kg, NP) with or without repeated intraperitoneal injection of A-83-01 (1 mg A-83-01/kg) into CDF1 mice bearing colon 26. Each value represents the mean ± SD ($n$ = 3).

Please note: Wiley-Blackwell are not responsible for the content or functionality of any supporting materials supplied by the authors. Any queries (other than missing material) should be directed to the corresponding author for the article.

# Development of an *in Vitro* Drug Release Assay of PEGylated Liposome Using Bovine Serum Albumin and High Temperature

Atsuko HIOKI, Ai WAKASUGI, Kumi KAWANO, Yoshiyuki HATTORI, and Yoshie MAITANI*

*Institute of Medicinal Chemistry, Hoshi University; 2–4–41 Ebara, Shinagawa-ku, Tokyo 142–8501, Japan.*
Received November 18, 2009; accepted June 19, 2010; published online June 21, 2010

**In this study, to establish the conditions of a drug release assay for PEGylated liposome formulations that relates with the drug stability profile in serum *in vivo*, the influences of incubation temperature and serum protein in the release buffer were examined using liposomal doxorubicin (DXR). In *in vitro* drug release assays, a PEGylated liposomal DXR in phosphate buffered saline (PBS) at 37 °C showed higher drug release rate than non-PEGylated formulation although PEGylated liposomal DXR had higher stability than an equivalent non-PEGylated formulation following intravenous injection. When bovine serum albumin (BSA) and increased temperature, 50 °C, were used to accelerate drug release from the liposomes and to mimic *in vivo* result, non-PEGylated liposomal DXR showed conversely higher release than a PEGylated formulation. Since high temperature increased BSA adsorption onto liposomes, BSA may cause non-PEGylated liposomes instability more than PEGylated ones, resulting in the reverse of the drug release rate of both liposomes. This finding suggested that the conditions in the drug release assay with PEGylated liposomal DXR may be able to be set by a combination of BSA and providing additional thermal energy.**

**Key words** PEGylated liposome; drug release assay; bovine serum albumin; stability; doxorubicin

To date, nano-sized systems such as liposomes have been explored for the systemic delivery of anti-cancer agents as potential drug delivery systems (DDS). The incorporation of polyethyleneglycol (PEG)-modified lipids (PEGylated) into liposomes efficiently overcomes problems associated with liposome elimination. Liposomal doxorubicin (Doxil®) is currently on the market. In order to rationally design liposomal DDS, it is necessary to fully characterize their drug retention and release properties both *in vitro* and *in vivo*. Several *in vitro* drug release assays of liposomes have been reported,[1—3] but there are few standards for drug release assays of liposome-based formulations at present. Furthermore, it is often the cases that *in vitro*-based drug release assays do not accurately predict the liposomal drug retention properties actually observed *in vivo*. PEGylated liposomes are not stable compared with non-PEGylated ones in buffer (pH 7.4) contrary to *in vivo* result that PEGylated liposomes is significantly stable in serum compared with non-PEGylated ones.[4—6]

For quality assessment as well as *in vivo* relevance; the possibility of *in vitro–in vivo* correlation, a condition on accelerated *in vitro* assay for routine quality control purpose are needed. PEGylated liposomes composed of lipids with high phase transition temperatures require a long time to evaluate the drug release profile because the drug release rate of these liposomes is quite slow. The addition of surfactants such as detergent has been applied,[7] however, some detergents might insert into liposomes during incubation and change the physicochemical properties of intact liposomes. $NH_4Cl$ and high sucrose in release buffer to compensate drug gradient inside liposome was added.[3,8] We used high temperature, 50 °C in release studies in spite of far from the physiological environment. This method will be effective in shortening the experimental time-period.

Serum is frequently added to the buffer to more closely mimic the physiological environment. We also used bovine serum albumin (BSA) as a serum protein since albumin was assumed to be comparatively readily adsorbed by liposomes *in vivo*.[9] This approach may be useful in research on the release profile of PEGylated liposomes although *in vitro* studies where PEGylated liposomes were incubated with only one type of protein could not be extrapolated directly to the more dynamic *in vivo* situation.

In this study, to establish conditions for a drug release assay corresponding of the release properties of a drug in liposomal formulations *in vivo*, the release profile of the formulations of liposomal doxorubicin was examined using BSA-containing buffer and increased temperature.

## MATERIALS AND METHODS

**Materials** Doxorubicin (DXR) hydrochloride, cholesterol (Ch), BSA, and Coomassie brilliant blue R-250 (CBB) were obtained from Wako Pure Chemical Industries, Ltd. (Osaka, Japan). Fully hydrogenated soy phosphatidylcholine (HSPC), distearoylphosphatidylcholine (DSPC) and polyethyleneglycol-distearoylphosphatidylethanolamine (PEG-DSPE, molecular weight of PEG: 2000) were purchased from NOF Co. (Tokyo, Japan). Other reagents used in this study were of reagent grade.

**Animal** Male ddY mice weighing 26—29 g were purchased from Sankyo Lab Service Co., Ltd. (Tokyo, Japan). The animal experiments were done under ethical approval from the Institutional Animal Care and Use Committee.

**Liposome Preparation** Lipid mixture (about 50 mg) was dissolved in chloroform in a round bottomed flask. To prepare a dried lipid film, chloroform was removed by rotary evaporation. The lipid films were subsequently hydrated in 3 ml of warm 300 mM citrate buffer (pH 4.0) for DXR encapsulation. Liposomes were subsequently sonicated by probe sonicator to reduce the size of about 100 nm. The mean diameter and $\zeta$-potential of the liposomes were determined by dynamic light scattering and electrophoresis methods, respectively (ELS-Z2, Otsuka Electronics Co., Ltd., Osaka, Japan) at 25 °C after diluting the liposome suspension with water.

* To whom correspondence should be addressed. e-mail: yoshie@hoshi.ac.jp

**Liposomal DXR** Six kinds of liposomal DXR were tested here; for liposomes composed of low Ch molar ratio (low Ch-liposome), HSPC/Ch/DSPC (60 : 20 : 20, DL), HSPC/Ch/PEG-DSPE (67 : 22 : 11, DSL), HSPC/Ch/PEG-DSPE (60 : 20 : 20, DSLh); for liposomes composed of high Ch molar ratio (high Ch-liposome), HSPC/Ch (56 : 44, DCL), HSPC/Ch/PEG-DSPE (54 : 42 : 4, DCSL), and HSPC/Ch/PEG-DSPE (52 : 40 : 8, DCSLh). The numbers in parentheses represents the molar % of each lipid. Low Ch- (L) and high Ch-liposomes (CL) each as part of non-PEGylated or PEGylated liposomes (S) are indicated as L, CL, SL, and CSL, respectively. Liposomal DXR is indicated as D. CLh and SLh stand for higher molar % of PEG-DSPE of CL and SL, respectively. The formulations of high Ch-liposomes were decided referring to Doxil®.[10] The formulation of low Ch-liposomes was increased PEG-DSPE because low PEG modification did not change release profiles in preliminary experiment. These liposomes were actively loaded with DXR by a pH gradient method as reported previously.[11] After the external pH was adjusted to pH 7.4, liposomes were incubated with DXR at a drug : total lipid ratio of 1 : 5 (w/w) at 60 °C for 25 min, and passed through a Sephadex-G50 column by eluting with saline to remove any unencapsulated DXR. To determine the encapsulation efficiency, the drug concentration was analyzed at $\lambda_{ex}$ 480/$\lambda_{em}$ 580 nm using a fluorescence spectrophotometer F-4010 (Hitachi Co., Ltd., Tokyo, Japan).

**Drug Release Experiments** Different liposomal formulations were diluted in two different release buffers, phosphate buffered saline (PBS) with or without 1% BSA, which corresponded to be used outside of dialysis tubing. One milliliter of diluted liposomes (200 $\mu$g DXR/ml) was placed into dialysis tubing (Spectra/Por CE, molecular weight cutoff of $M_r$=100 K, Spectrum Laboratories Inc., Rancho Dominguez, CA, U.S.A.), and dialyzed against 100 ml of release buffer. The condition may permit transport of the complex of released drug with BSA through dialysis membrane; effect of BSA binding on the dialysis membrane with respect to drug release may be neglected since free drug showed more than 60—80% release 3 h after incubation (data not shown). The dialysis process was performed at 37 °C and 50 °C and away from bright light. At various time points, 1 ml aliquots were withdrawn from the outer aqueous solution for analysis and replaced by 1 ml of fresh release medium. The samples were stored at 4 °C until analysis and fluorescence was quantified spectrophotometrically. Drug release profiles from liposome were expressed according to experimental equation:

$$\text{the percentage of drug released} = \frac{M_t}{M_0} \cdot 100 = Kd \cdot \sqrt{t}$$

Where $M_0$ is the total amount of drug in liposomes, $M_t$ is the amount of drug released at time $t$, and $Kd$ is the release rate constant (% $h^{-1/2}$). $Kd$ values will enable formulations to compare quantitatively the release profiles.

**Pharmacokinetic Analysis** Male ddY mice were given free or liposomal DXR by intravenous injection *via* the lateral tail vein in a single dose of 5 mg DXR/kg. At 4, 6, and 24 h after the injection, the mice were anesthetized by ether inhalation and immediately sacrificed by cervical dislocation. Blood was sampled first, and then liver and spleen were excised rapidly, rinsed in physiological saline, and weighed. Blood samples were centrifuged at 14000 rpm for 4 min at 4 °C to separate the serum. The serum and tissue samples were stored at −20 °C until analysis. DXR concentrations of serum and tissues were determined by the HPLC method.[12] Daunomycin (100 ng) was added to all samples as an internal standard. The HPLC system was composed of an LC-10$AT_{vp}$ pump (Shimadzu Co., Kyoto, Japan), a SIL-10A autoinjector (Shimadzu Co.), an RF-10$A_{XL}$ fluorescence detector ($\lambda_{ex}$ 482/$\lambda_{em}$ 550 nm, Shimadzu Co.), and an YMC-Pack ODS-A, 150×4.6 mm i.d. column (YMC Co., Ltd., Kyoto, Japan). The mobile phase was 0.1 M ammonium formate (pH 4.0) : acetonitrile=7 : 3 (v/v) at a flow rate of 1.0 ml/min. The concentration of DXR in each sample was determined using a calibration curve. The plasma area under the curve (*AUC*) from 0 to 24 h and clearance were calculated using the bootstrap method.[13]

**BSA Binding to Liposomes** Empty liposomes, CL, and CSLh (corresponding to 1 mg lipid) were incubated with 100 $\mu$l of 1% BSA solution for 3 and 8 h at 37 °C and 50 °C in assist tubes. The liposome suspensions were placed in centrifuge tubes and then diluted with 900 $\mu$l PBS. BSA solution was used as a control to exclude non-specific binding. The liposome suspensions were ultracentrifuged at 41000 rpm for 1 h at 25 °C, and the pellets were washed three times with PBS. BSA in the pellet was extracted with 100 $\mu$l of 2% sodium dodecyl sulfate (SDS) and analyzed by 10% SDS-polyacrylamide gel electrophoresis (SDS-PAGE) under reducing conditions. The gels were stained with Coumassie brilliant blue (CBB). BSA amounts were estimated by scanning the gel bands using Kodak 1D Image Analysis Software.

## RESULTS

**Liposome Characterization** Table 1 presents the particle size, entrapment efficiency, and $\zeta$-potentials of liposomal formulations. The results indicated that all liposomes had a size ranging from 93 to 120 nm. High Ch-liposomes, DCL and DCSL, showed an entrapment efficiency of >93%, but low Ch-liposomes, DL, showed an efficiency of about 60%. The entrapment efficiency of DL decreased when the amount of Ch in the formulation was low; furthermore, that in DSL was decreased by the PEG modification by 11—20 mol% compared with DL. DSL showed highly negative $\zeta$-potentials compared to the non-PEGylated formulations.

**Drug Release Studies** To examine the conditions of the

Table 1. Particle Size, Entrapment Efficiency and $\zeta$-Potential of Liposomal DXR

| Liposomes | Particle size (nm) | Entrapment efficiency (%) | $\zeta$-Potential (mV) |
|---|---|---|---|
| Low Ch-liposomes | | | |
| DL | 105.7±11.2 | 60.0±2.5 | −5.2±1.5 |
| DSL | 98.2±10.5 | 36.6±3.2 | −28.5±0.2 |
| DSLh | 92.5±9.7 | 40.2±2.3 | −29.4±0.8 |
| High Ch-liposomes | | | |
| DCL | 105.2±10.3 | 97.4±1.1 | −6.4±0.5 |
| DCSL | 109.8±10.5 | 93.8±1.5 | −25.3±0.4 |
| DCSLh | 118.5±4.2 | 95.2±0.8 | −26.1±1.2 |

Each value represents the mean±S.D. ($n$=3). DL and DCL represent low Ch-liposomes and high Ch-liposomes entrapped DXR, respectively. SL represents PEGylated liposome. SLh represents higher PEGylated liposome than each SL.

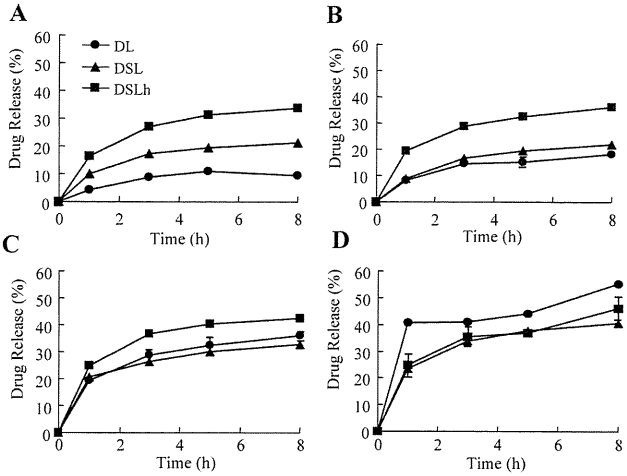


Fig. 1. Effect of Temperature and BSA (1%, w/v) in PBS Medium on the Release of DXR from DL and DSLh

Release experiments were performed using a dialysis method at 37 °C without (A) or with BSA (B), and at 50 °C without (C) or with BSA (D). Each value represents the mean±S.D. ($n$=3).

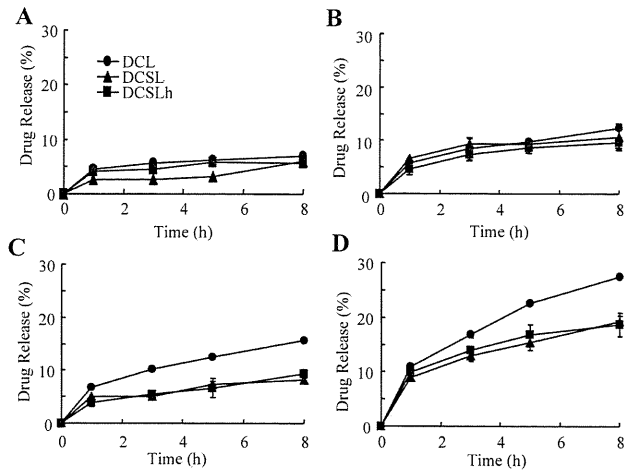


Fig. 2. Effect of Temperature and BSA (1%, w/v) in PBS Medium on the Release of DXR from DCL and DCSLh

Release experiments were performed using a dialysis method at 37 °C without (A) or with BSA (B), and at 50 °C without (C) or with BSA (D). Each value represents the mean±S.D. ($n$=3).

Table 2. The Release Rate Constant (*Kd*) of Liposomal DXR to Estimate Effect of Temperature and BSA on the *in Vitro* DXR Release Profiles in Figs. 1 and 2

| Condition | | *Kd* (% $h^{-1/2}$)[a] | | | *Kd* (% $h^{-1/2}$)[b] | | |
|---|---|---|---|---|---|---|---|
| Temp. (°C) | Medium | DL | DSL | DSLh | DCL | DCSL | DCSLh |
| 37 | PBS | 4.9 | 9.2 | 14.8 | 3.1 | 1.9 | 2.7 |
| 37 | +1% BSA | 7.5 | 9.0 | 15.8 | 4.5 | 4.8 | 4.0 |
| 50 | PBS | 15.8 | 14.9 | 19.9 | 5.7 | 3.1 | 3.2 |
| 50 | +1% BSA | 21.6 | 18.4 | 17.6 | 9.9 | 7.0 | 8.0 |

Each value shows the slope of the straight line with $r^2$>0.8. *a*) Calculated from *in vitro* DXR release profile of low Ch-liposomes in Fig. 1. *b*) Calculated from *in vitro* DXR release profile of high Ch-liposomes in Fig. 2.

drug release assay, low Ch-liposomes were incubated at 37 °C or 50 °C in PBS with or without 1% BSA. The profiles of DXR release from DL and DSL are shown in Fig. 1. After incubation at 37 °C in PBS for 8 h, DSLh, DSL, and DL showed about 30%, 20%, and 10% release, respectively. When the % drug release of liposomes was plotted as a function of the square of time, the plot showed linearity until 5 h at an early stage (correlation $r^2$ with >0.8, data not shown) where the slope *Kd* calculated (Table 2). The *Kd* values of DL, DSL, and DSLh were 4.9, 9.2, and 14.8% $h^{-1/2}$. After incubation at 37 °C or 50 °C in PBS with or without BSA, an increase in the release rate was seen with all liposomes compared with those in only PBS (Fig. 1C). At 50 °C, DL was mostly influenced by the presence of BSA and the *Kd* (21.6% $h^{-1/2}$) of DL became conversely higher than those of DSL (18.4% $h^{-1/2}$) and DSLh (17.6% $h^{-1/2}$) (Fig. 1D).

The profiles of DXR release from high Ch-liposomes, DCL and DCSL are shown in Fig. 2. After incubation at 37 °C with 1% BSA and 50 °C in PBS for 8 h, the difference in the release rate was not significant except for DCL (Figs. 2A—C). After incubation at 50 °C in PBS with BSA, DCL showed the highest release rate (Fig. 2D). The *Kd* values of DCL, DCSL, and DCSLh were similar after incubation at 37 °C in PBS with or without BSA, and rose to 9.9, 7.0 and 8.0% $h^{-1/2}$ at 50 °C in PBS with BSA, respectively (Table 2). No change in the particle size of DCL or DCSL was observed after the release assay. Precipitation was not seen except a little cloudiness when BSA was added to the release buffer. Similar to DL, even increase of Ch amount in liposomes, DCL was mostly influenced at 50 °C by the presence of BSA and became higher release. These findings suggest that PEG moiety may protect liposomes from change of circumstance by addition of BSA and increased buffer's temperature.

***In Vivo* Drug Concentration after Intravenous Injection** To examine the correlation of the drug release properties of liposomes *in vitro* and *in vivo*, DCL and DCSLh were selected. Figure 3 shows the *in vivo* drug concentration profiles of free and liposomal DXR after intravenous injection in mice. Serum clearance kinetics of DCSLh was compared to that of free DXR and DCL. As shown in Fig. 3A, clearance of DCSLh (0.13±0.03 ml/h; mean±S.D.) was 222 and 3.4 times lower than that of free DXR and DCL, respectively. *AUC* value of DCSLh, DCL and free DXR in serum was 1263±391 μg·h/ml, 362±95 μg·h/ml and 5.2±0.3 μg·h/ml, respectively. The tissue distribution of liposomal DXR was also examined (Figs. 3B, C). DCL accumulated 21.8% of the injected DXR dose in both the liver and the spleen at 6 h. DCSLh accumulated only 12.5% of the injected DXR dose in both the liver and the spleen at 6 h. As a result, DCSLh maintained higher stability in the bloodstream compared to DCL. Although the DXR levels in the bloodstream contained both liposomal DXR and free DXR released, the released

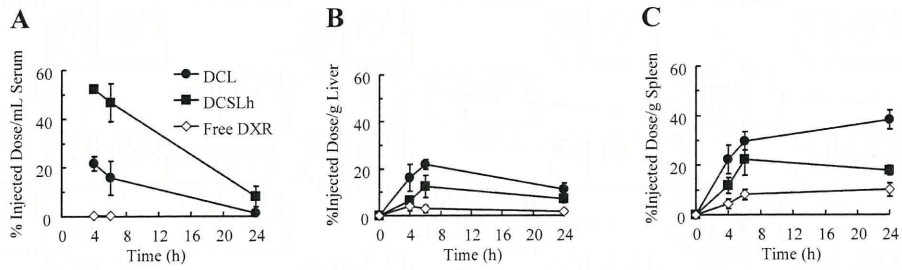


Fig. 3. DXR Levels in Serum (A), Liver (B), and Spleen (C) after Intravenous Injection of DCL, DCSLh and Free DXR into ddY Mice at a Dose of 5 mg DXR/kg

Each value represents the mean±S.D. ($n$=4).

free DXR is very rapidly cleared from the bloodstream and therefore, the detected DXR in blood was considered to be mainly the liposomal one after intravenous injection in this study.

**BSA Binding to Liposomes** To clarify the influence of temperature and BSA on the drug release profile of PEGylated liposomes, BSA adsorbed onto empty liposomes (CL and CSLh) during incubation was evaluated by SDS-PAGE. As shown in Fig. 4, a band of BSA, as observed in the 1% BSA solution, was not present in the sample. The amount of BSA adsorbed to CL and CSLh-8 at 37 °C increased with an increase in incubation time; 9 and 80 $\mu$g BSA/mg lipid for CSLh and 7 and 50 $\mu$g BSA/mg lipid for CL at 3 and 8 h, respectively, indicating that slightly less BSA absorbed to PEGylated CSLh than to non-PEGylated CL. These adsorbed amounts were near that for dipalmitoylphosphatidylglycerol liposomes (58 $\mu$g/mg) incubated in BSA solutions at 37 °C for 1 h.[14] Moreover, at 3 h the amount of BSA adsorbed at 50 °C increased to approximately 250 and 280 $\mu$g BSA/mg lipid for CL and CSLh, respectively.

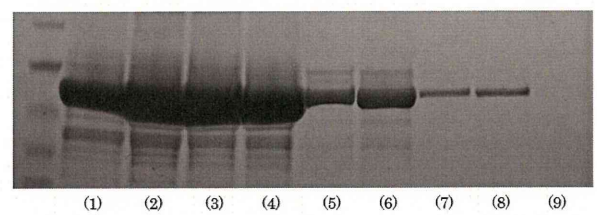


Fig. 4. CBB-Stained SDS-Polyacrylamide Gel (10%) of BSA Adsorbed onto Liposomes

Empty liposomes (corresponding to 1 mg lipid) were incubated in 1% (w/v) BSA (100 $\mu$l) for either 3 or 8 h at 37 °C or 50 °C. (1) CSLh and (2) CL were incubated for 8 h at 50 °C (3) CSLh and (4) CL were incubated for 3 h at 50 °C, (5) CSLh and (6) CL were incubated for 8 h at 37 °C, (7) CSLh and (8) CL were incubated for 3 h at 37 °C, and (9) 1%BSA solution.

## DISCUSSION

The drug release rate from liposomes may be affected by the preparation method of liposomes,[6] vesicle size,[9,15] formulation[15—17] and loading method of the drug,[6] *etc.* Here, all liposomes were prepared by the thin film method, the particle diameter was adjusted to about 100 nm by sonication, and loading method of the drug was same among the formulations. Six liposomal formulations were tested where the Ch content was high and low and with or without PEGylated lipids. In addition, the relation of the *in vivo* stability of liposomes in the bloodstream with the drug release profile *in vitro* was examined. Furthermore, influence of temperature and BSA on PEGylated and non-PEGylated liposomes in a release assay was evaluated by measuring the adsorption amount of BSA.

In PEGylated low Ch-liposomes with 11 and 20 mol% of PEG-DSPE, the particle size tended to be smaller. This finding may be explained as PEG increasing the repulsive forces on the liposome surface with negatively charged PEG-DSPE.[18] PEGylated low Ch-liposomes decreased the encapsulation efficacy of DXR. It was thought that PEG chain in the aqueous inner part in liposomes may decrease the volume of water inside liposomes,[14] and the PEG conformational model changes liposomes.[19] PEGylated high Ch-liposomes did not change the encapsulation efficacy. DXR seemed to be highly encapsulated by liposomes as the Ch content increased, which was probably concerned with the addition of Ch to the phospholipid membrane resulting in stabilization of the membrane and related to maintenance of the pH gradient during encapsulation.[11]

In the drug release test, both low and high Ch-liposomes exhibited similar profiles. BSA is homologous to human serum albumin (HSA) in terms of its functions, and BSA did not suffer unfolding at 50 °C.[20] After incubation at 37 °C in PBS, the drug release from both liposomes increased with the increase in PEG modification. It is thought that PEG modification may cause liposome instability and the rapid release of encapsulated drugs. To the contrary, in high temperature and the addition of BSA, the drug release from non-PEGylated liposomes became higher than PEGylated ones. This finding corresponded well to the report that the release of fluorescence entrapped in liposomes in PBS was slow, but when BSA or serum was added the release rate increased.[21—23] It was reported that the adsorption of BSA brings about a phase separation in liposomes and that a temporary gap is consequently formed in the liposomal bilayer membranes, thereby the permeability of liposomal bilayer membranes increases by the adsorption of BSA.[23]

The difference in the serum DXR levels following systemic administration of DCL and DCSLh is contributed by the difference in the release profiles of these liposomes in the blood stream and the difference in their capture by the liver and spleen. At an early stage postinjection, it may be greatly affected by the former. Enhancement of their stability *in vivo* was explained that the steric barrier of PEG prevents the aggregation of colloidal carriers,[24] and prevents protein adsorption in serum with the increase in the water-binding

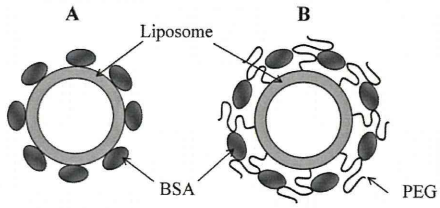


Fig. 5. Schematic Model for the Adsorption of BSA on Non-PEGylated Liposomes (A) and PEGylated Liposomes (B)

(A) After incubation with PBS containing BSA. BSA probably penetrates into the bilayer center, and the adsorption of BSA caused an increase in the permeability of the membranes. (B) PEG immobilized on the surface of PEGylated liposomes may prevent the direct interaction of BSA with liposomes.

ability of the PEG chains.[25—27] Therefore, the effect of adsorption of BSA onto liposomes was examined in terms of the stability of liposomes *in vitro*.

The amount of BSA adsorption to the liposomes was increased in line with the incubation time and temperature. At 50 °C, the amount of BSA adsorbed to the liposomes, CL and CSL, increased greatly to almost the same level at 3 h incubation. The difference in the drug release profile of DCL and DCSL may be due to differences in the adsorption site of BSA rather than the adsorption amount. The adsorption of BSA on non-PEGylated CL might bring about an increase in the permeability of liposomal bilayer membranes (Fig. 5A).[21] On the other hand, in the case of PEGylated CSL, BSA might be trapped in the intermolecules of the PEG chain and not interact directly with the liposome, which resulted in protection of the surface of the liposome (Fig. 5B). As a result, BSA stabilized CSL but destabilized CL. This difference in the stability of liposomes by adsorption of BSA was reflected in a large difference in the release profiles at 50 °C where the adsorption of BSA was increased. It was reported that the profiles of adsorbed proteins on PEGylated and non-PEGylated liposomes incubated in 10% serum were similar by SDS-PAGE.[7]

This finding corresponded well on our previous report that PEGylated liposome adsorbed HSA exhibited longer circulation in mice than only PEGylated ones.[28] PEG may not completely prevent interactions with serum proteins. PEG may form a shroud on the surface of the liposomes partially shielding hydrostatic charges,[24,29] but this may still allow for protein interactions with the surface of the liposome. Thus, this is the first report that a combination of BSA and temperature may act synergistically to increase the release of DXR from non-PEGylated liposomes compared with PEGylated liposomes *in vitro*. This may provide a good relation with the stability of PEGylated and non-PEGylated liposomes *in vitro* and in serum. In different loading method of the drug, we confirmed that this condition also worked release of fluorescence entrapped during formation of liposomes (data not shown).

## CONCLUSION

In *in vitro* drug release assays, PEGylated liposomes could be more stable than non-PEGylated liposomes in both the presence of BSA and at high temperature because adsorbed BSA may cause non-PEGylated liposomes instability more than PEGylated ones. Thus, the conditions of the drug release assay of PEGylated liposomal DXR might be able to replicate *in vivo* conditions, in which PEGylated liposomes exhibited more stable drug profile in serum than non-PEGylated liposomes, using a combination of BSA and by providing additional thermal energy.

**Acknowledgments** This study was supported in part by the Japan Health Sciences Foundation, by the Ministry of Education, Culture, Sports, Science and Technology of Japan, and by the Open Research Center Project.

## REFERENCES

1) Allen T. M., Cleland L. G., *Biochim. Biophys. Acta*, **597**, 418—426 (1980).
2) Peschka R., Dennehy C., Szoka F. C. Jr., *J. Controlled Release*, **56**, 41—51 (1998).
3) Shabbits J. A., Chiu G. N., Mayer L. D., *J. Controlled Release*, **84**, 161—170 (2002).
4) Han H. D., Choi M. S., Hwang T., Song C. K., Seong H., Kim T. W., Choi H. S., Shin B. C., *J. Pharm. Sci.*, **95**, 1909—1917 (2006).
5) Zhao X. B., Muthusamy N., Byrd J. C., Lee R. J., *J. Pharm. Sci.*, **96**, 2424—2435 (2007).
6) Calvagno M. G., Celia C., Paolino D., Cosco D., Iannone M., Castelli F., Doldo P., Frest M., *Curr. Drug Deliv.*, **4**, 89—101 (2007).
7) Assadullahi T. P., Hamid K., Hider R. C., *J. Microencapsul.*, **9**, 317—327 (1992).
8) Cui J., Li C., Guo W., Li Y., Wang C., Zhang L., Zhang L., Hao Y., Wang Y., *J. Controlled Release*, **118**, 204—215 (2007).
9) Price M. E., Cornelius R. M., Brash J. L., *Biochim. Biophys. Acta*, **1512**, 191—205 (2001).
10) Tardi P. G., Boman N. L., Cullis P. R., *J. Drug Target.*, **4**, 129—140 (1996).
11) Dos Santos N., Cox K. A., McKenzie C. A., van Baarda F., Gallagher R. C., Karlsson G., Edwards K., Mayer L. D., Allen C., Bally M. B., *Biochim. Biophys. Acta*, **1661**, 47—60 (2004).
12) Matsushita Y., Iguchi H., Kiyosaki T., Tone H., Ishikura T., Takeuchi T., Umezawa H., *J. Antibiot.*, **36**, 880—886 (1983).
13) Takemoto S., Yamaoka K., Nishikawa M., Takakura Y., *Drug Metab. Pharmacokinet.*, **21**, 458—464 (2006).
14) Blume G., Cevc G., *Biochim. Biophys. Acta*, **1146**, 157—168 (1993).
15) Mayer L. D., Tai L. C., Ko D. S., Masin D., Ginsberg R. S., Cullis P. R., M. Bally B., *Cancer Res.*, **49**, 5922—5930 (1989).
16) Hathout R. M., Mansour S., Mortada N. D., Guinedi A. S., *AAPS PharmSciTech.*, **8**, 1—12 (2007).
17) Anderson M., Omri A., *Drug Deliv.*, **11**, 33—39 (2004).
18) Garbuzenko O., Barenholz Y., Priev A., *Chem. Phys. Lipids*, **135**, 117—129 (2005).
19) Nicholas A. R., Scott M. J., Kennedy N. I., Jones M. N., *Biochim. Biophys. Acta*, **1463**, 167—178 (2000).
20) Aoki K., "Serum Albumin," Kodansha, Tokyo, 1984.
21) Tsunoda T., Imura T., Kadota M., Yamazaki T., Yamauchi H., Kwon K. O., Yokoyama S., Sakai H., Abe M., *Colloids Surf. B Biointerfaces*, **20**, 155—163 (2001).
22) Funato K., Yoda R., Kiwada H., *Biochim. Biophys. Acta*, **1103**, 198—204 (1992).
23) Yokouchi Y., Tsunoda T., Imura T., Yamauchi H., Yokoyama S., Sakai H., Abe M., *Colloids Surf. B Biointerface*, **20**, 95—103 (2001).
24) Ahl P. L., Bhatia S. K., Meers P., Roberts P., Stevens R., Dause R., Perkins W. R., Janoff A. S., *Biochim. Biophys. Acta*, **1329**, 370—382 (1997).
25) Sadzuka Y., Nakade A., Hirama R., Miyagishima A., Nozawa Y., Hirota S., Sonobe T., *Int. J. Pharm.*, **238**, 171—180 (2002).
26) Woodle M. C., *Adv. Drug Deliv. Rev.*, **32**, 139—152 (1998).
27) Mercadal M., Domingo J. C., Petriz J., Garcia J., de Madariaga M. A., *Biochim. Biophys. Acta*, **1418**, 232—238 (1999).
28) Watanabe M., Kawano K., Toma K., Hattori Y., Maitani Y., *J. Controlled Release*, **127**, 231—238 (2008).
29) Woodle M. C., Newman M. S., Cohen J. A., *J. Drug Target.*, **2**, 397—403 (1994).

# Increase of the therapeutic effect by treating nasopharyngeal tumor with combination of HER-2 siRNA and paclitaxel

YOSHIYUKI HATTORI, MOTOKI HAKOSHIMA, KIMIKO KOGA and YOSHIE MAITANI

Institute of Medicinal Chemistry, Hoshi University, Shinagawa-ku, Tokyo 142-8501, Japan

Received November 26, 2009; Accepted January 22, 2010

DOI: 10.3892/ijo_00000585

**Abstract.** Therapeutic agents targeting HER-2/neu have been intensively addressed over the past decades. Previously, we reported that HER-2 synthetic small interfering RNA (HER-2 siRNA) could suppress the growth of human nasopharyngeal KB tumor xenografts by intratumoral injection with lipid-based nanoparticles; however, complete regression of the tumor was not achieved. In this study, we investigated anti-tumor activity by RNA interference in combination with paclitaxel (PTX) for KB cells using HER-2 siRNA and HER-2 short hairpin RNA-expressing plasmid DNA (HER-2 shRNA pDNA). Suppression of HER-2 expression by siRNA or shRNA pDNA caused significant reduction of proliferation by inducing apoptosis and enhancing the sensitivity for PTX in HER-2 positive KB cells. Interestingly, an HER-2 antibody trastuzumab could not increase the antitumor effect by PTX in KB xenografts. Combination therapy by intratumoral injection of HER-2 siRNA or HER-2 shRNA pDNA with PTX significantly inhibited the tumor growth of xenografts compared with each therapy used individually. In particular, HER-2 shRNA pDNA plus PTX largely extended the mean survival days compared with HER-2 siRNA plus PTX. Collectively, these findings suggest that HER-2 shRNA-based combined therapy with PTX could be a novel strategy to inhibit the progression of HER-2-positive cancer.

## Introduction

The HER-2 proto-oncogene (c-erbB-2/neu) belongs to the epidermal growth factor (EGF) receptor family and has been implicated in malignant transformation (1). HER-2 is thought to play an important role in tumorigenesis, DNA repair, drug resistance, and metastasis. HER-2 gene expression has been found to be amplified and/or overexpressed in breast (2), ovarian (3), lung (4), prostate (5), thyroid (6) and pancreatic cancers (7). HER-2 overexpression induced the down-regulation of p53 protein through the PI3 K/AKT pathway (8), leading to increased cell proliferation and decreased sensitivity to chemotherapeutic drugs (9); therefore, HER-2 has become an important target for cancer therapy.

Interference with HER-2 mRNA translation could be more effective than blockade of the already expressed HER-2 on the cell surface by HER-2 antibody. Specific down-regulation of HER-2 expression in tumors by ribozyme (10-12), antisense DNA (13-15), small interfering synthetic siRNA nucleotide (siRNA) (16,17), plasmid DNA (pDNA) encoding a short hairpin RNA (shRNA pDNA) (18) and antisense RNA/sense DNA hybrid duplexes (19) have been reported. Successful down-regulation of HER-2 will require sustained and high transfection of the therapeutic gene. RNA interference (RNAi) is a post-transcriptional mechanism of gene silencing mediated by cleavage of target RNA. RNAi has potential not only as a tool in biological analysis, but also as an evolutional drug for cancer gene therapy. In RNAi technology, two delivery systems were considered; direct delivery of siRNA, and introduction of shRNA pDNA that will be enzymatically degraded into siRNA. Synthetic siRNAs, which are 21-28 bp small double-stranded RNA, are substrates for the RNA-induced silencing complex.

In a previous study, we reported that HER-2 synthetic small interfering (HER-2) siRNA could suppress the growth of human nasopharyngeal KB tumor xenografts by intratumoral injection with lipid-based nanoparticles (NP) (20); however, complete regression of the tumor was not observed. Recently, it has been reported that combination therapy with HER-2 antibody trastuzumab and paclitaxel (PTX) is useful for the clinical treatment of breast cancer (21-23). Thus, it was expected that combination therapy with HER-2 siRNA and chemotherapy would be effective; however, it has not been reported in *in vivo* models. Therefore, in the present study, we evaluated the potential of HER-2 siRNA and HER-2 short hairpin RNA-expressing plasmid DNA (HER-2 shRNA pDNA) using NP delivery to increase the therapeutic efficacy of PTX in HER-2-positive KB cells and tumor xenografts.

## Materials and methods

*Synthetic siRNA.* The stealth RNA interference duplex-targeting nucleotides of HER-2 mRNA (HER-2 siRNA) and stealth RNAi Negative Control kit with Medium GC as a control for HER-2 siRNA (Cont siRNA) were synthesized by Invitrogen (Carlsbad, CA, USA). The sequences of HER-2 siRNA were as follows: HER-2 sense, 5'-AAACGUGUCUG

*Correspondence to*: Dr Yoshiyuki Hattori, Institute of Medicinal Chemistry, Hoshi University, Shinagawa-ku, Tokyo 142-8501, Japan
E-mail: yhattori@hoshi.ac.jp

*Key words:* synthetic siRNA, cationic nanoparticles, nasopharygeal tumor, HER-2

UGUUGUAGGUGACC-3'; HER-2 antisense, 5'-GGUCAC CUACAACACAGACACGUUU-3'.

*shRNA expressing plasmid DNA.* HER-2 shRNA pDNA encoding 21 mer shRNA against HER-2 with a hairpin-loop under the control of the U6 promoter (HuSH 19-21 mer shRNA construct against ERBB2) was obtained from OriGene Technologies, Inc. (MD, USA). The targeted sequences of HER-2 shRNA pDNA was as follows: HER-2 sense, 5'-AGTGAGCACCATGGAGCTGGC-3'; HER-2 antisense, 5'-GCCAGCTCCATGGTGCTCACT-3'. The pRS-shGFP (29) non-effective plasmid (Cont shRNA pDNA, OriGene Technologies, Inc.) was used as a negative control. A protein-free preparation of these plasmids was purified following alkaline lysis using the EndoFree Plasmid Max kit (Qiagen, Hilden, Germany).

*Cell culture.* Human nasopharyngeal tumor KB cells were supplied by the Cell Resource Center for Biomedical Research, Institute of Development, Aging and Cancer, Tohoku University (Miyagi, Japan). Human cervix epithelial adenocarcinoma HeLa cells were obtained from the European Collection of Cell Culture (Wiltshire, UK). Human lung carcinoma A549 cells were a gift from Oncotherapy Science (Tokyo, Japan). KB and A549 cells were grown in RPMI-1640 medium (Invitrogen) and HeLa cells in Eagle's Minimum Essential Medium (Invitrogen), supplemented with 10% heat-inactivated fetal bovine serum (FBS, Invitrogen) and kanamycin (100 $\mu$g/ml) at 37°C in a 5% $CO_2$ humidified atmosphere.

*In vitro and in vivo transfection.* For *in vitro* and *in vivo* transfections of siRNA and shRNA pDNA, we used lipid-based nanoparticles (NP) as previously reported (20,24). For *in vitro* transfection, NP was mixed with 100 pmol siRNA or 2 $\mu$g shRNA pDNA in the presence of 50 mM NaCl solution at a charge ratio (+/-) of 3/1. The NP and siRNA or shRNA pDNA complex (nanoplex) was kept at room temperature for 15 min. The nanoplex was diluted with culture medium containing 10% FBS and transfected into cells at a final concentration of 100 nM siRNA or 2 $\mu$g/ml shRNA pDNA in the medium.

For *in vivo* transfection, NP was mixed with 10 $\mu$g siRNA or shRNA pDNA in water at a charge ratio (+/-) of 1/1. The nanoplex was kept at room temperature for 15 min. Male BALB/c nu/nu mice (6-8 weeks of age) were purchased from CLEA Japan Inc. (Tokyo, Japan). To generate KB tumor xenografts, $1x10^7$ cells suspended in 50 $\mu$l RPMI medium were inoculated subcutaneously into the mice. The tumor volume was calculated using the formula, tumor volume = 0.5 x a x $b^2$, where a and b are the larger and smaller diameters, respectively. When the average volume of KB xenograft tumors reached about 100 $mm^3$, the nanoplex of siRNA or shRNA pDNA was directly injected into xenografts.

*Antiproliferative activity.* KB, A549 and HeLa cells were seeded in 96-well plates 24 h prior to transfection. Cells at 30% confluence in the wells were transfected with siRNA or shRNA pDNA by NP and then incubated for 72 h. In combined treatment of siRNA or shRNA pDNA with paclitaxel (PTX, Wako, Osaka, Japan), the cells were incubated for 48 h after transfection of siRNA or shRNA pDNA, and then treated with various concentrations of PTX for another 48 h. Cell viability (%) was measured by the WST-8 assay (Dojindo Laboratories, Kumamoto, Japan) as previously reported (25).

*Western blot analysis.* KB, A549 and HeLa cells were seeded in a 35-mm culture dish 24 h before transfection. The cells were transfected with HER-2 siRNA or HER-2 shRNA pDNA, and then incubated for 48 h. Cell protein extracts were prepared with sampling buffer containing 1% Triton X-100 in phosphate-buffered saline (PBS), pH 7.4. After they were centrifuged at 10,000 x g for 10 min, the protein concentration of the supernatant was quantitated with the bicinchonic acid protein assay reagent (Pierce, Rockford, IL, USA). For the detection of ß-actin protein, 10 $\mu$g protein was separated by 12.5% SDS-PAGE, and for the detection of HER-2 protein, 10 $\mu$g protein was separated by 7.5% SDS-PAGE. They were then transferred to a polyvinylidene difluoride (PVDF) membrane (FluoroTrans® W, PALL Gelman Laboratory, Ann Arbor, MI, USA). Membranes were blocked in PBS containing 0.1% Tween-20 with 5% skimmed milk at 37°C for 1 h. The blot of HER-2 protein was probed with rabbit anti-human HER-2 antibody (Lab Vision, Fremont, CA, USA). Goat anti-rabbit IgG peroxidase conjugate (Santa Cruz Biotechnology, Inc., Santa Cruz, CA, USA) was used as a secondary antibody. Blots of ß-actin protein were probed with a mouse anti-human ß-actin IgG peroxidase conjugate [ß-actin (C4) HRP, Santa Cruz Biotechnology, Inc.]. Immunoblots were detected using a SuperSignal West Pico Chemiluminescent Substrate (Pierce).

*Caspase 3/7 activities.* KB and A549 cells were seeded in a 35-mm culture dish and incubated overnight. Cells at 30% confluence in the wells were transfected with siRNA or shRNA pDNA by NP for 24 h. For measuring caspase 3/7 activity, a homogeneous assay (Caspase-Glo™ 3/7 assay, Promega, Madison, WI, USA) was performed as previously reported (25).

*In vivo therapy.* In gene therapy by transfection of HER-2 siRNA or HER-2 shRNA pDNA alone, the nanoplexes of 10 $\mu$g siRNA or 10 $\mu$g shRNA pDNA per tumor were directly injected into xenografts on days 0, 2 and 4. In the combined therapy of trastuzumab with PTX, trastuzumab (Herceptin, Chugai Pharmaceutical Co., Ltd., Tokyo, Japan) at a dose of 20 mg/kg and PTX at a dose of 5 mg/kg were simultaneously injected i.p. and i.v., respectively, on day 0, 3, 6 and 9. In the combined therapy of HER-2 siRNA or HER-2 shRNA pDNA with PTX, nanoplexes of 10 $\mu$g siRNA or 10 $\mu$g shRNA pDNA per tumor were directly injected into xenografts on days 0, 3, 6 and 9, and PTX at a dose of 5 mg/kg was injected i.v. on day 1, 4, 7 and 10. Tumor volume and mean survival days were measured. The data are shown as the mean ± SD. Animal experiments were conducted with ethics approval from our institutional animal care and use committee.

*Statistical analysis.* Statistical differences between different groups were analyzed with one-way analysis of variance on ranks with Tukey-Kramer's post-hoc test. A $p \leq 0.05$ was considered significant. For the animal study, statistical comparison was performed by Student's t-test.

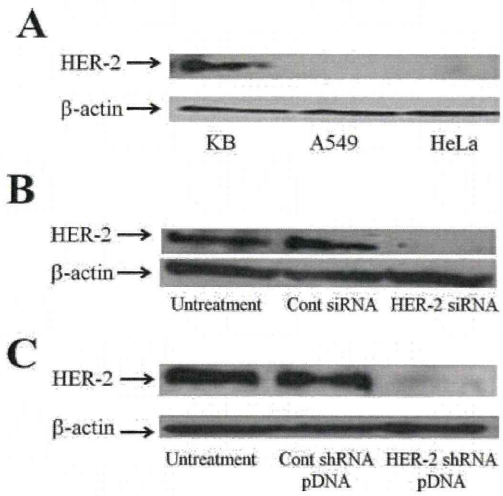


Figure 1. HER-2 expression in KB, A549 and HeLa cells (A) and suppression of HER-2 expression by transfection of HER-2 siRNA (B) or HER-2 shRNA pDNA (C) in KB cells. Expression of HER-2 protein was detected by Western blot analysis 48 h after transfection.

## Results

*Suppression of HER-2 protein by gene knockdown.* HER-2 protein is a well-known protein overexpressed in many tumors and is related to apoptosis and cell growth (1). First, we investigated the expression of HER-2 mRNA in KB, A549 and HeLa cells by Western blot analysis (Fig. 1A). HER-2 protein was strongly expressed in KB cells, but not detected in A549 and HeLa cells; therefore, in subsequent experiments, we used KB cells as a HER-2 positive cell line, and A549 and HeLa cells as HER-2 negative cell lines.

Next, we confirmed the decreased expression of HER-2 protein by transfecting HER-2 siRNA or HER-2 shRNA pDNA into KB cells. In this study, we used lipid-based nanoparticles (NP) for siRNA and shRNA pDNA transfection as previously reported (20,24,26). When transfected into KB cells, HER-2 siRNA or HER-2 shRNA pDNA strongly inhibited the expression of HER-2 protein, but did not affect the expression of ß-actin (Fig. 1B and C). Control constructs, Cont siRNA and Cont shRNA pDNA, did not affect the expression either HER-2 or ß-actin protein in the cells.

*Antiproliferative activity.* We examined cell viability by WST-8 assay 48 h after transfection of HER-2 siRNA and HER-2 shRNA pDNA into KB, A549 and HeLa cells. In the transfection of HER-2 siRNA and HER-2 shRNA pDNA, a decrease of cell viability was significantly observed in KB cells, but not in A549 and HeLa cells (Fig. 2A and B). In contrast, Cont siRNA and Cont shRNA pDNA did not affect cell viability in KB, A549 and HeLa cells.

Next, to examine the effect of HER-2 suppression on the activity of apoptosis-associated enzymes, we measured caspase 3/7 activity 48 h after transfection with HER-2 siRNA or HER-2 shRNA pDNA (Fig. 2C and D). Transfection of HER-2 siRNA and HER-2 shRNA pDNA in KB cells increased caspase 3/7 activities about 1.4- and 1.5-fold higher than those of Cont siRNA and Cont shRNA pDNA,

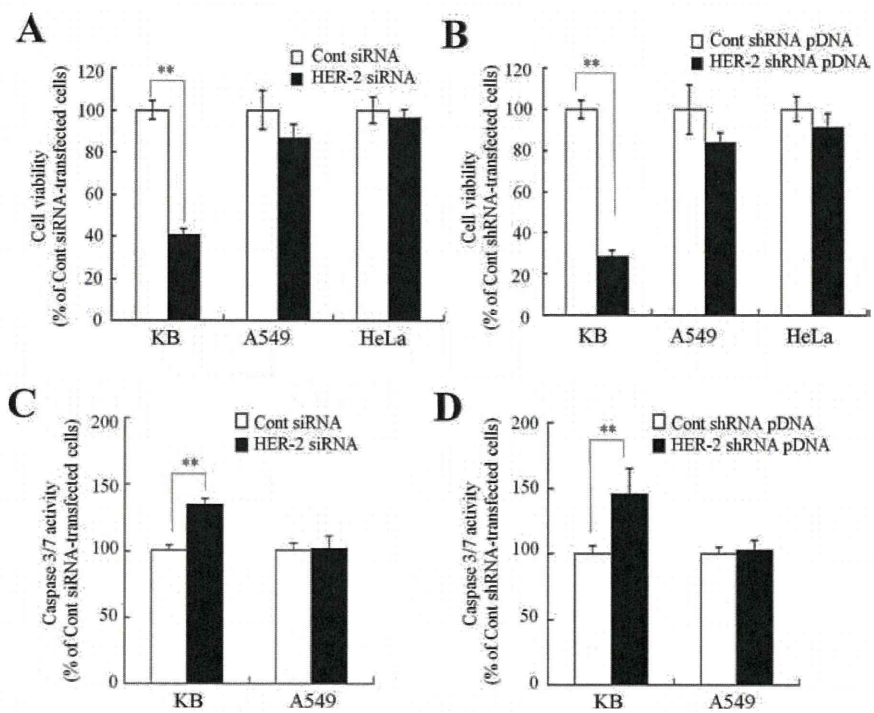


Figure 2. Antiproliferative and caspase 3/7 activities 48 h after transfection of HER-2 siRNA or HER-2 shRNA pDNA into cells. After transfection with HER-2 siRNA or HER-2 shRNA pDNA, cell viability in KB, A549 and HeLa cells (A and B) and caspase 3/7 activity in KB and A549 cells (C and D) were measured. Each column shows the mean ± SD (n=3). $^{**}P<0.01$, compared with Cont siRNA in A and C, and with Cont shRNA pDNA in B and D.

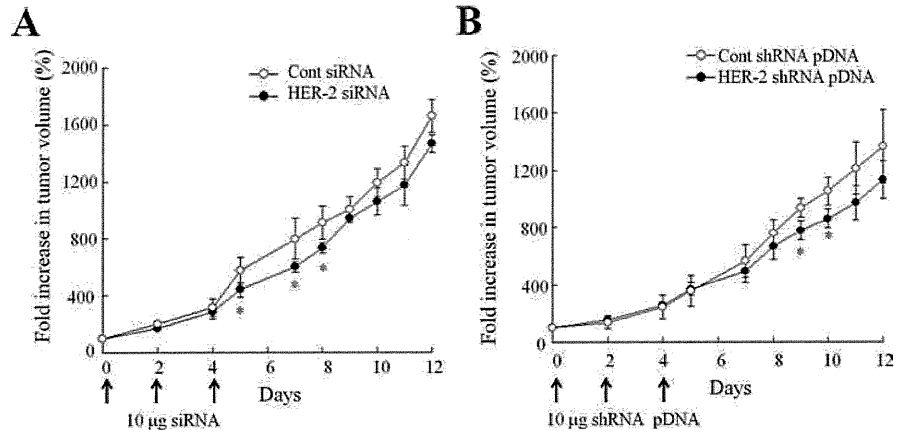


Figure 3. *In vivo* gene therapy of KB tumor xenografts. siRNA (A) or shRNA pDNA (B) was injected directly into the tumor three times (day 0, 2 and 4). The results are the mean ± SE (n=4-6). $^{*}P<0.05$, compared with Cont siRNA in A and with Cont shRNA pDNA in B.

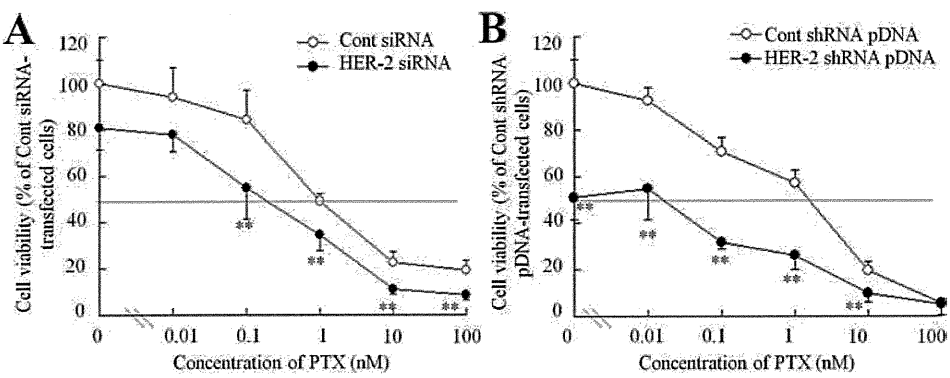


Figure 4. Dose effect of PTX on cytotoxicity in KB cells in the presence of siRNA (A) or shRNA pDNA (B). KB cells were transfected for 48 h with siRNA or shRNA pDNA. The cells were treated with various concentrations of PTX and incubated for another 48 h. The number of viable cells was determined by WST-8 assay, n=4 for each sample. $^{*}P<0.05$ and $^{**}P<0.01$, compared with Cont siRNA in A and with Cont shRNA pDNA in B.

respectively ($p<0.01$), whereas did not increase activity in A549 cells. These results suggested that HER-2 siRNA and HER-2 shRNA pDNA induced the inhibition of cell growth via apoptosis in HER-2-positive cells.

*In vivo gene therapy in KB tumor xenografts.* We evaluated the antitumor effect by direct injection into KB tumor xenografts with the nanoplex of HER-2 siRNA or HER-2 shRNA pDNA. *In vivo* transfections of siRNA and shRNA pDNA were performed three times as previously reported (20). In mice treated with HER-2 siRNA, the growth of KB tumors was significantly inhibited on day 5, 7 and 8 compared with mice treated with Cont siRNA (Fig. 3A). In mice treated with HER-2 shRNA pDNA, growth was significantly inhibited on day 9 and 10 compared with mice treated with Cont shRNA pDNA (Fig. 3B). The time of tumor suppression by HER-2 shRNA pDNA seemed to be delayed more than that of HER-2 siRNA. However, sustained suppression of tumor growth was not observed in the xenografts after injection of HER-2 siRNA and HER-2 shRNA pDNA. HER-2 activates cell survival pathways, which represents an advantage for tumor cells as they became resistant to chemotherapy-induced apoptosis (8). Down-regulation of HER-2 expression in tumor cells via activation of the apoptosis pathway will enhance cytotoxicity by chemotherapy; therefore, for complete tumor regression, combination therapy with HER-2 siRNA and chemotherapy was examined.

*In vitro combination therapy with PTX.* It has been reported that the HER-2 antibody trastuzumab enhances the antitumor activity of PTX against HER-2-overexpressing human breast cancer xenografts (27), and combination therapy with trastuzumab and PTX has been useful for the clinical treatment of breast cancer (21-23). Therefore, we evaluated the *in vitro* growth inhibitory effect by the combination of HER-2 siRNA or HER-2 shRNA pDNA with PTX. Forty-eight hours after the transfection of siRNA or shRNA pDNA into KB cells, the cells was treated with PTX for another 48 h. Cells transfected with HER-2 siRNA showed 3.2-fold higher sensitivity to PTX ($IC_{50}$=0.3 nM) than those transfected with Cont

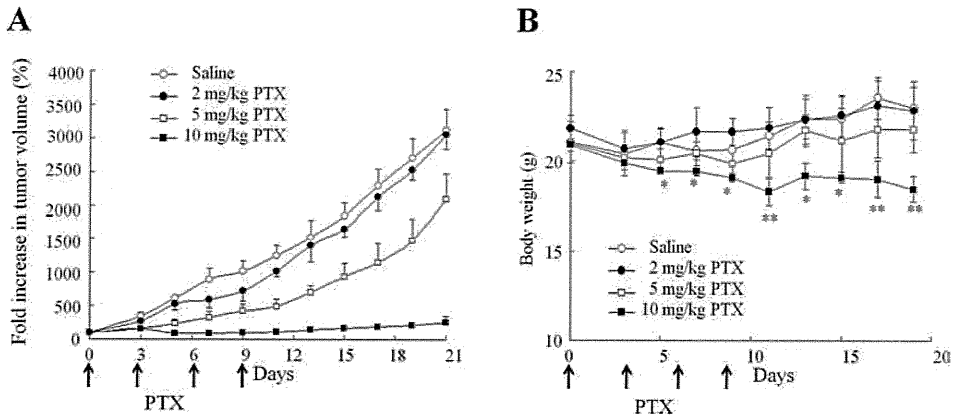


Figure 5. Dose-dependent effect of PTX on antitumor effect (A) and body weight change (B) for KB tumor xenografts. PTX was injected i.v. at a dose of 2, 5 and 10 mg/kg on days 0, 3, 6 and 9. Tumor volume (A) and body weight change (B) were measured after starting treatment. Data are the mean ± SE, n=3 for each group. $^{*}P<0.05$ and $^{**}P<0.01$; compared with mice injected with saline.

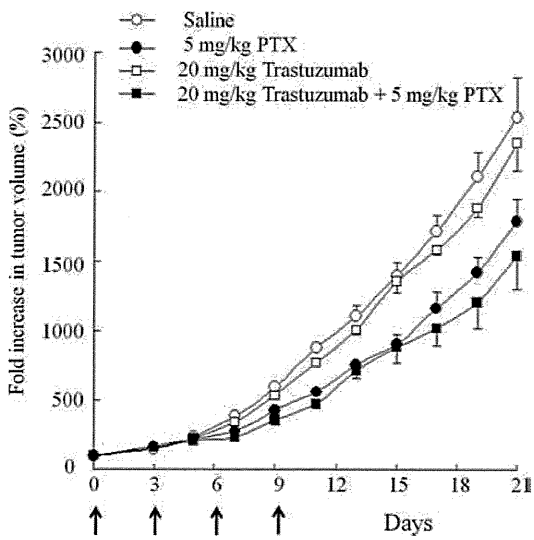


Figure 6. *In vivo* combination therapy of trastuzumab and PTX for KB tumor xenografts. When the average volume of KB tumor xenografts reached 100 $mm^3$ (day 0), trastuzumab at 20 mg/kg (i.p.) and/or PTX (i.v.) at 5 mg/kg were injected on days 0, 3, 6 and 9. n=3 for each group.

siRNA ($IC_{50}$=0.97 nM) (Fig. 4A). Cells transfected with HER-2 shRNA pDNA showed 92.5-fold higher sensitivity to PTX ($IC_{50}$=0.03 nM) than those with Cont shRNA pDNA ($IC_{50}$=2.7 nM) (Fig. 4B). These data indicated that suppression of HER-2 expression may increase sensitivity to PTX.

*Combined therapy for KB tumor xenografts.* To determine the optimal dose of PTX to evaluate combination therapy *in vivo*, PTX was administered at doses of 2, 5 and 10 mg/kg, 4 times at three-day intervals. The tumor suppressive effect by PTX was dose-dependent; 5 mg/kg PTX inhibited the tumor growth of KB xenografts moderately but not at 2 mg/kg (Fig. 5A). There were no significant differences in mouse body weight changes after PTX administration at doses of 2 and 5 mg/kg; however, body weight at 10 mg/kg PTX significantly decreased as a side effect (Fig. 5B); therefore, we decided to use 5 mg/kg PTX for the following combination therapy.

First, we investigated whether HER-2 inhibition by trastuzumab enhanced the antitumor activity of PTX for KB tumor xenografts. Trastuzumab was simultaneously i.p. injected at a dose of 20 mg/kg, as previously reported (28), on days 0, 3, 6 and 9 along with PTX; however, trastuzumab treatment alone could not inhibit tumor growth, and the combination with PTX could not significantly enhance the antitumor effect by PTX (Fig. 6).

Next, we evaluated the efficacy of combination therapy of HER-2 siRNA or HER-2 shRNA pDNA plus PTX in inhibiting the growth of KB tumors. Nanoplexes of 10 $\mu$g HER-2 siRNA or HER-2 shRNA pDNA per tumor were directly injected into xenografts four times (days 0, 3, 6 and 9). PTX was intravenously administered at a dose of 5 mg/kg 24 h after the injections of nanoplexes (days 1, 4, 7 and 10). HER-2 siRNA or HER-2 shRNA pDNA treatment alone could not suppress tumor growth, but HER-2 siRNA and HER-2 shRNA pDNA with PTX treatment significantly suppressed tumor growth on day 7, 9 and 11, and day 9, 11 and 13, respectively, compared with PTX treatment alone (Figs. 7A and 8A). The median survival time with HER-2 siRNA combined treatment (31.5 days) was slightly longer than with HER-2 siRNA (28.5 days) or PTX (30.0 days) alone (Fig. 7B). The median survival time with HER-2 shRNA pDNA combined treatment (42.5 days) largely extended than that of the HER-2 shRNA pDNA (32.0 days) or PTX (35.0 days) alone (Fig. 8B). Transfection with siRNA, shRNA pDNA, PTX injection (5 mg/kg) alone, or their combinations did not alter the change in body weight during 3 weeks of treatment (data not shown). These data suggested that combination therapy of PTX with HER-2 siRNA or HER-2 shRNA pDNA was more effective than that of PTX with trastuzumab.

## Discussion

Previously, we reported that NP-delivered HER-2 siRNA suppressed HER-2 expression, but insufficiently inhibited KB tumor growth (20). In this study, we investigated the anti-

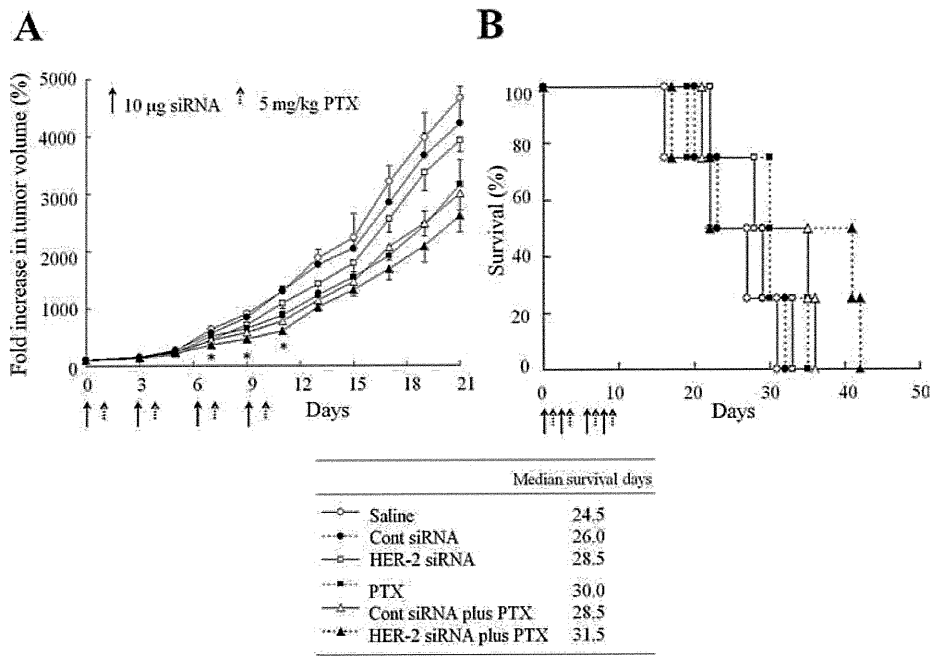


| | Median survival days |
|---|---|
| Saline | 24.5 |
| Cont siRNA | 26.0 |
| HER-2 siRNA | 28.5 |
| PTX | 30.0 |
| Cont siRNA plus PTX | 28.5 |
| HER-2 siRNA plus PTX | 31.5 |

Figure 7. *In vivo* combination therapy of HER-2 siRNA and PTX for KB tumor xenografts. When the average volume of KB tumor xenografts reached 100 $mm^3$ (day 0), HER-2 or Cont siRNA were directly injected into the tumor four times (days 0, 3, 6 and 9). PTX at a dose of 5 mg/kg was injected i.v. four times (days 1, 4, 7 and 10). Tumor volume (A) and mean survival days (B) were measured after starting treatment. In A, data are shown as the mean ± SE. n=3 for each group. *P<0.05; compared with mice injected with PTX.

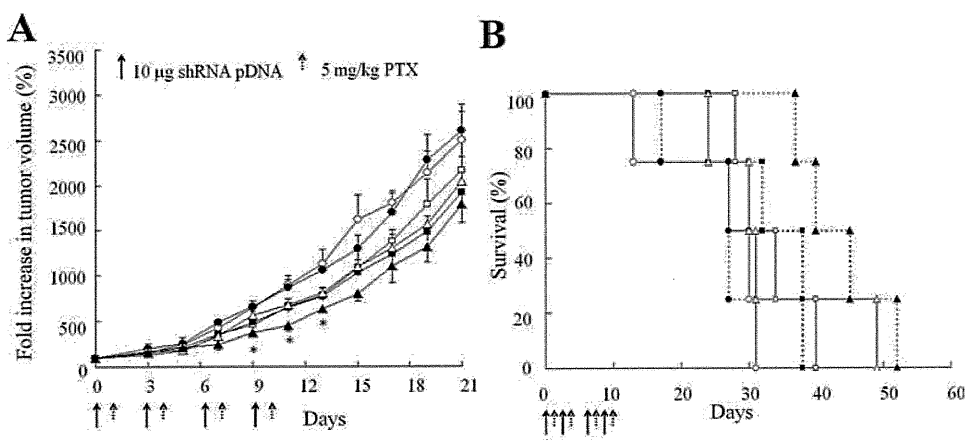


| | Median survival days |
|---|---|
| Saline | 28.5 |
| Cont shRNA pDNA | 27.0 |
| HER-2 shRNA pDNA | 32.0 |
| PTX | 35.0 |
| Cont shRNA pDNA plus PTX | 30.5 |
| HER-2 shRNA pDNA plus PTX | 42.5 |

Figure 8. *In vivo* combination therapy with HER-2 shRNA pDNA and PTX for KB tumor xenografts. Experimental conditions were the same as in Fig. 7.

tumor effect of NP transfection of HER-2 shRNA pDNA compared with HER-2 siRNA into KB cells and tumor xenografts. Furthermore, we examined their combination therapy with PTX.

The intracellular localization of HER-2 siRNA and HER-2 shRNA pDNA after transfection is crucial for its successful function. A difference in time of the antitumor effect between HER-2 siRNA and HER-2 shRNA pDNA was slightly observed (Fig. 3). In combination therapy with PTX, HER-2 shRNA pDNA exhibited marked extension of mean survival days compared with HER-2 siRNA (Figs. 7B and 8B). HER-2 siRNA can quickly trigger specific degradation of HER-2 mRNA after transfection into cytoplasm. On the other hand, HER-2 shRNA pDNA must be transferred into the nucleus